frontiers | Frontiers in Molecular Biosciences

TYPE Original Research
PUBLISHED 14 May 2025
DOI 10.3389/fmolb.2025.1597130

OPEN ACCESS

EDITED BY
Daniel X. Zhang,
Hong Kong Metropolitan University, Hong Kong SAR, China

REVIEWED BY
Larance Ronsard,
Ragon Institute, United States
Charly Abi Ghanem,
Albany Medical College, United States

*CORRESPONDENCE
Teresa A. Milner,
tmilner@med.cornell.edu
Michael J. Glass,
mjg2003@med.cornell.edu

†These authors have contributed equally to this work and share first authorship

‡These authors have contributed equally to this work and share senior authorship

RECEIVED 20 March 2025
ACCEPTED 22 April 2025
PUBLISHED 14 May 2025
CORRECTED 01 September 2025

CITATION
Marongiu R, Platholi J, Park L, Yu F, Sommer G, Woods C, Milner TA and Glass MJ (2025) Promotion of neuroinflammation in select hippocampal regions in a mouse model of perimenopausal Alzheimer's disease. *Front. Mol. Biosci.* 12:1597130. doi: 10.3389/fmolb.2025.1597130

Promotion of neuroinflammation in select hippocampal regions in a mouse model of perimenopausal Alzheimer's disease

Roberta Marongiu[1,2,3†], Jimcy Platholi[1,4†], Laibaik Park[1], Fangmin Yu[1], Garrett Sommer[1], Clara Woods[1], Teresa A. Milner[1*‡] and Michael J. Glass[1*‡]

[1]Feil Family Brain and Mind Research Institute, Weill Cornell Medicine, New York, NY, United States, [2]Neurological Surgery Department, Weill Cornell Medicine, New York, NY, United States, [3]Genetic Medicine Department, Weill Cornell Medicine, New York, NY, United States, [4]Anesthesiology Department, Weill Cornell Medicine, New York, NY, United States

Introduction: Alzheimer's disease, the most common form of dementia, is characterized by age-dependent amyloid beta (Ab) aggregation and accumulation, neuroinflammation, and cognitive deficits. Significantly, there are prominent sex differences in the risk, onset, progression, and severity of AD, as well as response to therapies, with disease burden disproportionately affecting women. Although menopause onset (i.e., perimenopause) may be a critical transition stage for AD susceptibility in women, the role of early ovarian decline in initial disease pathology, particularly key neuroinflammatory processes, is not well understood.

Methods: To study this, we developed a unique mouse model of perimenopausal AD by combining an accelerated ovarian failure (AOF) model of menopause induced by 4-vinylcyclohexene diepoxide (VCD) with the 5xFAD transgenic AD mouse model. To target early stages of disease progression, 5xFAD females were studied at a young age (~4 months) and at the beginning stage of ovarian failure analogous to human perimenopause (termed "peri-AOF"), and compared to age-matched males. Assessment of neuropathology was performed by immunohistochemical labeling of Ab as well as markers of astrocyte and microglia activity in the hippocampus, a brain region involved in learning and memory that is deleteriously impacted during AD.

Results: Our results show that genotype, AOF, and sex contributed to AD-like pathology. Aggregation of Ab was heightened in female 5xFAD mice and further increased at peri-AOF, with hippocampal subregion specificity. Further, select increases in glial activation also paralleled Ab pathology in distinct hippocampal subregions. However, cognitive function was not affected by peri-AOF.

Discussion: These findings align with the hypothesis that perimenopause constitutes a period of susceptibility for AD pathogenesis in women.

KEYWORDS

amyloid beta, astrocyte, microglia, ovarian failure, pyramidal cell

Introduction

Dementia is a leading contributor to the global burden of disease (Alzheimer's disease facts and figures, 2023) with Alzheimer's disease (AD) constituting approximately 50%–70% of cases (Alzheimer's, 2016). AD is characterized by progressive neurodegeneration and cognitive dysfunction (Arvanitakis et al., 2019; Zhang et al., 2024). A main hallmark of AD neuropathology is the accumulation of parenchymal plaques containing aggregated amyloid-beta (Aβ) in the cerebral cortex and the hippocampal formation (Braak and Braak, 1991). In addition to Aβ deposition, AD involves a complex set of related neurodegenerative processes including neuroinflammation (Lista et al., 2024). In AD animal models, neuroinflammation characterized by the activation of reactive astrocytes and microglia (Raz et al., 2016) is one of the earliest pathological manifestations, likely contributing to synaptic and neuronal loss.

Important sex differences in AD are well documented, with women experiencing a disproportionately greater disease burden (Kolahchi et al., 2024). The incidence of AD is at least two-fold higher in women compared to men (Alzheimer's, 2016) with women exhibiting faster disease progression (Pike, 2017) and greater cognitive impairment at comparable stages of AD (Laws et al., 2016). Perimenopause, the transitional phase of irregular gonadal hormonal production and cycling before full menopause, may be a particularly vulnerable period for the onset of mild cognitive impairment and AD. This is supported by evidence that low endogenous estrogen levels are associated with increased AD risk (Gong et al., 2022), and that early or late age at menopause is associated with an elevated or decreased risk for AD, respectively (Liao et al., 2023; Wedatilake et al., 2024; Steventon et al., 2023). Furthermore, there is growing evidence that initiating estrogen replacement soon after menopause may help mitigate dementia development (Mills et al., 2023). Significantly, perimenopause is also associated with declines in brain volume (Mosconi et al., 2018) and increases in Aβ expression (Mosconi et al., 2018; Mosconi et al., 2017). Despite these associations, the mechanisms underlying the heightened perimenopausal risk for AD, particularly those related to neuroinflammation and cognitive decline in the hippocampus, remain unclear.

Animal models may help elucidate the mechanisms driving perimenopausal AD risk. The commonly used 5xFAD transgenic mouse model, which expresses five familial mutations in two AD risk genes, exhibits increased Aβ production and plaque formation that parallels AD pathology (Oakley et al., 2006). Notably, sex differences have been reported in 5xFAD mice, with females showing earlier increases in inflammatory gene expression (Manji et al., 2019), glial markers (Sil et al., 2022; Islam et al., 2024) as well as Aβ levels (Manji et al., 2019; Sil et al., 2022; Bhattacharya et al., 2014). This neuropathology correlates with worse cognitive performance, in some studies (Manji et al., 2019; Sil et al., 2022; Islam et al., 2024), but not all (Ganesh et al., 2024; O'Leary et al., 2020). Markers of brain inflammation appear as early as 3 months of age, suggesting that sex differences in AD-like pathology emerge at a prodromal stage (Manji et al., 2019). Additionally, female 5xFAD mice show increased hippocampal Aβ and elevated expression of immune-related genes and proteins compared to age-matched males (Oakley et al., 2006; Bundy et al., 2019; Blasco Tavares Pereira Lopes et al., 2022; Poon et al., 2023; Sadleir et al., 2015; Maarouf et al., 2013). These sex differences may be linked to changes in estrogen signaling (Prange-Kiel et al., 2016; Kubota et al., 2016; Quinn et al., 2022). Thus, combining mouse models of AD with perimenopause in females may help to isolate the effects of hormonal changes on AD neuropathology.

The 4-vinylcyclohexene diepoxide (VCD) ovatoxin mimics perimenopause in rodents by producing accelerated ovarian failure (AOF) paralleling the irregular hormone fluctuations seen during human perimenopause (termed "peri-AOF" in rodents) before transitioning to full menopause (Van Kempen et al., 2014; Brooks et al., 2016; Marques-Lopes et al., 2017). This model allows for controlled induction of AOF at various times/ages following sexual maturity in younger animals, reducing the confounding effects of chronological aging, a main AD risk factor (Van Kempen et al., 2014; Brooks et al., 2016; Marques-Lopes et al., 2017). The VCD model has been used to investigate how ovarian failure influences metabolic (Abi-Ghanem et al., 2025; Abi-Ghanem et al., 2024; Gannon et al., 2023), aging (Golub et al., 2008), and cerebrovascular (Blackwell et al., 2022) factors to influence cognitive function, brain plasticity and amyloid pathology in wild-type (WT) mice or in mouse models of cognitive impairment and dementia. However, the impact of early ovarian failure (peri-AOF) on Aβ-related pathology and neuroinflammatory response in 5xFAD mice is unknown.

We investigated whether peri-AOF contributes to hippocampal neuroinflammation in young 5xFAD mice treated with VCD. A granular assessment of Aβ levels and glial markers of neuroinflammation was conducted by analyzing all major hippocampal subfields at rostral and caudal levels. Cognitive performance was assessed using tests of learning and memory. To characterize early AD-like neuropathology, we focused on young (~4 months) 5xFAD mice. Age-matched male mice were also tested to evaluate the effect of biological sex.

Experimental procedures

Animals

Young adult [~2 month-old at the initiation of the experiments (Flurkey and Currer, 2004)] C57BL/6 WT mice (n = 22 females and n = 11males) and transgenic 5xFAD (C57BL/6 background; n = 22 female and n = 11 male) mice were bred and maintained in a colony at Weill Cornell Medicine (WCM). Breeding pairs of hemizygous 5xFAD mice were obtained from the Jackson Laboratory (Bar Harbor, ME; JAX MMRRC stock#034840). Mice were bred in-house and genotyped prior to experimentation.

Abbreviations: Aβ, beta amyloid; AD, Alzheimer's disease; AOF, accelerated ovarian failure; cCA1, caudal CA1; Cen, central hilus; cDG, caudal DG; DG, dentate gyrus; GFAP, glial fibrillary acidic protein; Iba1, ionized calcium binding adapter molecule 1; IFG, infragranular blade; PB, phosphate buffer; PCL, pyramidal cell layer; rCA1, rostral CA1; rDG, rostral DG; SG, supragranular blade; SLM, stratum lacunosum-moleculare; SLu, stratum lucidum; SO, stratum oriens; SR, stratum radiatum; TS, Tris saline; VCD, 4-vinylcyclohexene diepoxide.

5xFAD mice express human APP and PSEN1 transgenes with a total of five AD-linked mutations under the control of the Thy1 promoter. This mouse model exhibits early-onset parenchymal Aβ aggregation correlated with cognitive deficits (Xu et al., 2014a; Richard et al., 2015). Amyloid deposition begins in the cerebral parenchyma at 2–3 months of age, with little accumulation in the cerebral vasculature, and amyloid plaques are found throughout the hippocampus and cortex by 6 months (Oakley et al., 2006; Xu et al., 2014b). Astrogliosis and microgliosis begin around 2 months, developing in parallel with plaque deposition (Oakley et al., 2006). Mice were housed in groups of three to four animals per cage and maintained on a 12-h light/dark cycle (lights out 18:00 h) with *ad libitum* access to water and rodent chow. At euthanasia, mice weighed 23–32 g. All experiments were approved by the WCM Institutional Animal Care and Use Committees and followed the National Institutes of Health guidelines for the Care and Use of Laboratory Animals guidelines.

AOF model of perimenopause

AOF induction by VCD treatment in mice has been shown to recapitulate the gradual hormonal fluctuations that correspond to peri- and post-menopause in humans (reviewed in (Van Kempen et al., 2011; Marques-Lopes et al., 2018)). The AOF model can be used to separate hormonal effects from aging effects and can be applied to any mouse genotype (Van Kempen et al., 2014; Brooks et al., 2016; Marques-Lopes et al., 2017). Low dose VCD injections selectively deplete ovarian primary follicles without negatively affecting peripheral tissues, kidney, or liver function (Brooks et al., 2016; Haas et al., 2007; Sahambi et al., 2008; Wright et al., 2008). VCD does not directly increase inflammation markers in the brain, including the hippocampus (Van Kempen et al., 2014).

AOF induction

Gonadally intact 53-58-postnatal-day-old female mice received 130 mg/kg VCD (cat. #S453005 Millipore Sigma, St. Louis, MO) in sesame oil (cat. # 8008-74-0 Millipore Sigma) for 5 days per week for 3 weeks (Marques-Lopes et al., 2017; Van Kempen et al., 2011). Control mice received injections of sesame oil only. Prior studies from our lab and others (Van Kempen et al., 2014; Haas et al., 2007; Lohff et al., 2005) established the peri-AOF stage as occurring 58 days after the first VCD injection. At this stage (~3.5 months old), the mice exhibit irregular, prolonged estrous cycles and elevated plasma follicle stimulating hormone (Lohff et al., 2005; Mayer et al., 2004; Harsh et al., 2007). Behavioral assessments of VCD- and oil-treated females, as well as aged-matched males, were initiated when mice were about 4 months of age (the peri-AOF stage of VCD mice). A timeline of the experimental procedures is shown in Figure 1.

Estrous cycle assessment

At euthanasia, vaginal smears (Turner and Bagnara, 1971) were collected to determine the terminal estrous cycle stage via cytological examination. Estrous cycle phases were classified as proestrus (high estrogen), estrus (declining estrogen), or diestrus (low estrogen and progesterone). Most females were in estrus or diestrus at euthanasia.

Antibodies

4G8: A mouse monoclonal antibody raised against amino acid residues 17-24 of beta-amyloid (4G8, Biolegend Cat. # 800701) was employed. This antibody recognizes abnormally processed isoforms as well as precursor APP forms (manufacturer's instructions), and labels both parenchymal and vascular Aβ aggregates (Kövari et al., 2013; Alafuzoff et al., 2009; Marazuela et al., 2022; Davis et al., 2004). GFAP: A rabbit polyclonal antibody (Abcam # ab7260; lot # GR20948-21; RRID:AB_305808) raised against full-length human GFAP was used. On Western blot, this antibody recognized 48 kDa and 55 kDa GFAP bands (manufacturer's datasheet). Iba1: A rabbit polyclonal antibody raised against a synthetic peptide corresponding to the C-terminus of Iba1 (#SAR6502; 019-19741 FUJIFILM Wako Pure Chemical Corporation) was employed. The antibody reacts with rat, mouse and human Iba1 and recognizes a 17 kDa band protein on Western blot (manufacturer's datasheet). These antibodies have been used in our prior studies (Milner et al., 2022; Platholi et al., 2023).

Brain fixation and histology

Mouse brains were processed for immunocytochemistry using established procedures in our labs (Milner et al., 2011). Briefly, mice were deeply anesthetized with sodium pentobarbital (150 mg/kg, i. p.), and then perfused with saline. The brains were extracted, bisected sagittally, and the right hemisphere fixed in 4% paraformaldehyde in 0.1 M phosphate buffer (PB, pH 7.4) for 24 h on a shaker (70 rpm) at 4°C. The forebrain containing the hippocampus was sectioned (40 µm thick) on a vibratome (VT1000X Leica Microsystems, Buffalo Grove, IL) and stored in cryoprotectant (30% sucrose, 30% ethylene glycol in PB) at −20°C until immunocytochemical processing.

For each experiment, one rostral (−2.00 to −2.70 mm from Bregma (Hof et al., 2000)) or caudal (−2.90 to −3.50 mm from Bregma (Hof et al., 2000)) hippocampal section per animal was selected and then punch coded in the cortex. Tissue sections from each experimental group were pooled into single containers to ensure identical reagent exposure (Milner et al., 2011).

Light microscopic immunocytochemistry

Hippocampal sections from each genotype/sex group were processed for 4G8, Iba1 or GFAP (n = 11/group). Sections were rinsed in 0.1 M Tris-saline (TS; pH 7.6), blocked with 0.5% bovine serum albumin (BSA) in TS for 30 min, and incubated in primary antibodies mouse anti-4G8 (1:4000), rabbit anti-GFAP (1:6000) or rabbit anti-Iba-1 (1:4000) diluted in 0.1% Triton-X and 0.1% BSA in TS for 24-h at room temperature followed by 24-h at +4°C.

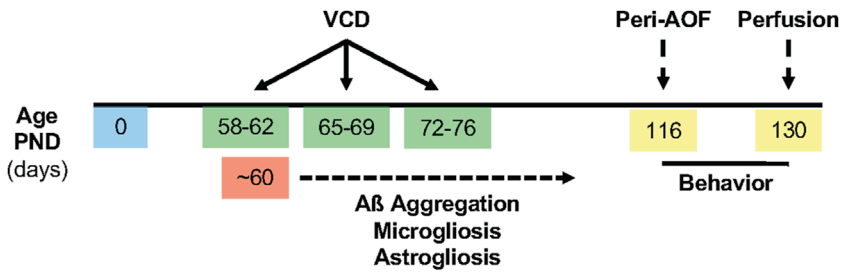

FIGURE 1
Timeline of experimental procedures. VCD (130 mg/kg, i. p.) was injected for 3 weeks, 5 days per week beginning between postnatal day (PND) 53-58. The extracellular deposition of Aß plaques was expected to begin at ~ PND 60, accompanied by microgliosis and astrogliosis. Behavioral assessments were performed for 2 weeks following the initiation of the peri-AOF phase. Brains were harvested at ~ PND 130.

Next, sections were rinsed in TS and incubated in either biotin-conjugated goat anti-rabbit IgG (for GFAP and Iba1; #111-065-144, Jackson ImmunoResearch Inc., West Grove, PA; RRID:AB_2337965) or goat anti-mouse IgG (for 4G8; # 115-065-166, Jackson ImmunoResearch Inc.; RRID:AB_2338569) in 0.1% BSA and TS. Sections were washed in TS and incubated in Avidin Biotin Complex (ABC; Vectastain Elite kit, Vector Laboratories, Burlingame, CA) at half the manufacturer's recommended dilution for 30-min. After rinsing in TS, the bound peroxidase was visualized by reaction in 3,3′-diaminobenzidine (Sigma-Aldrich, St. Louis, MO) and 0.003% hydrogen peroxide in TS for 6-min (4G8), 3-min (GFAP), or 8-min (Iba1). All primary and secondary antibody incubations were carried out at 145 rpm, whereas rinses were at 90 rpm on a rotator shaker. Sections were mounted in 0.05 MPB onto gelatin-coated glass slides, dehydrated through an ascending series of alcohol to xylene, and coverslipped with DPX (Sigma-Aldrich).

Image acquisition and field densitometry

Quantification for 4G8, Iba1 and GFAP labeling in the hippocampus were performed using previously established densitometric methods (Pierce et al., 2014; Williams and Milner, 2011; Williams et al., 2011). To ensure unbiased data quantification, the analysis was performed by investigators blinded to experimental conditions. Images were acquired using a Nikon Eclipse 80i microscope with a Micropublisher 5.0 digital camera (Q-imaging, BC, Canada) and IP Lab software (Scanalytics IPLab, RRID: SCR_002775). ImageJ64 software (ImageJ, RRID:SCR_003070) was used to measure the pixel density within regions of interest (ROI) in defined hippocampal subregions. ROIs within four subregions of the rostral and caudal hippocampus were selected: 1) CA1: stratum oriens (SO), pyramidal cell layer (PCL), stratum radiatum (SR) and stratum lacunosum-moleculare (SLM); 2) CA2/3a: SO, PCL, near and distal SR; 3) CA3b: SO, PCL, stratum lucidum (SLu) and SR; 4) Dentate gyrus (DG): the supragranular blade (SG), the infragranular blade (IFG) and the central hilus (Cen) and 5) Subiculum (caudal section). Background pixel density from non-labeled regions (e.g., corpus callosum) was subtracted to control for illumination variability and background labeling. Prior studies (Pierce et al., 2014) demonstrated a strong correlation between pixel density and actual transmittance, confirming measurement accuracy.

Behavioral assessments

Mice were tested sequentially over 2 weeks in the Novel Object Recognition, Y maze, and Barnes maze tasks, as described in prior studies (Park et al., 2020; Park et al., 2008). The same investigator conducted all behavioral tests. Testing occurred at the same time each day, with results recorded using ANY-maze (Stoelting Co.). Mice were habituated to the testing room for 2 h daily for 5 days before testing. On testing days, mice were acclimated to the room for 1-h before each session. The order of the Y-maze and Novel Object tests were counterbalanced, with 24-h rest between the tests. Behavioral apparatuses were cleaned with 70% ethanol between trials.

Y-maze

This test was used to assess spatial working memory as previously described (Milner et al., 2011). Mice were placed in a three-arm maze (40 cm long, 9.5 cm high, 4 cm wide) diverging at a 120° from the central point, and allowed to explore two arms for 5 min (training). After 30 min, the previously blocked arm was opened, serving as the novel arm (test trial). The sequence of arm entries (spontaneous alternation) and locomotor activity were recorded for 5 min. A Spontaneous alternation was defined as entities into all the 3 arms on consecutive occasions, and was manually recorded from the recorded videos. The total number of arms entered during the sessions, which reflect locomotor activity, also was recorded. The maximum alternation was subsequently calculated by measuring the total number of arm entries minus 2 and the percentage of alternation was calculated as ((actual alternation/maximum alternation)×100).

Novel object recognition (NOR)

The NOR apparatus (height 30 cm × width 28 cm × length 46 cm) consisted of an open field chamber with dim illumination throughout, and it is used to measure spatial and working memory. On day 1 (habituation phase), each mouse was allowed to explore the empty arena for 5-min. On day 2 (familiarization phase), two identical objects (type A) were placed on the floor of the area and the mouse was allowed to explore for 5-min followed by a 30-min rest. For the exploration phase, One of the type A objects was replaced with a novel object (type B) and the mouse was allowed to explore for 5-min the familiar and novel objects at the same

time. For each phase, the total distance traveled, the average speed, the total object exploration time, and the time spent exploring each one of the two objects was recorded. A discrimination index for day 2 exploration phase was calculated as percentage time spent exploring the novel object out of the total object exploratory time.

Barnes maze

The apparatus consisted of a maze with a 10 cm cylindrical white start chamber in the middle, multiple hole and one escape hole in the periphery. Mice were trained in the apparatus for four sequential days. Each training day consisted of 4 trials (with 15 min inter-trial intervals) in the following sequence: 1) Adaption period. The mouse was placed in the white start chamber, and a buzzer was switched on for 10-s. Following, the mouse was guided to an escape hole for 15-20-s. The buzzer was turned off and the mouse was allowed to stay in the escape box for 2-min 2) Spatial acquisition period. The mouse was placed in the start chamber and the buzzer was switched on for 10 s. After 10 s, the start chamber was removed, and the mouse was allowed to move around the maze to find an escape hole (maximum 3-min).

Immediately after the mouse entered the escape hole, the buzzer was turned off and the mouse was allowed to stay in the tunnel for 1-min. The average values collected from the spatial acquisition period of all four trials in a given training day is used as datapoint in the figures.

Twenty-four hours after the last training session, mice underwent the probe trial. For this, the mouse was placed in the maze in the white chamber and the buzzer was switched on. After 10-s, the chamber was removed, and the mouse behavior was recorded for 90-s. For each mouse, the latency time, errors, total length traveled to find the escape hole were recorded.

Image adjustments for figures

Images were adjusted first for contrast and sharpness in Adobe Photoshop 9.0 (Adobe Photoshop, RRID:SCR_014199). Next, images were imported into Microsoft PowerPoint, where final adjustments to brightness, sharpness and contrast were achieved. Images of different groups in the same figure were similarly adjusted to same brightness and contrast. Adjustments were made to the entire image, none of which significantly altered the appearance of the initial raw image.

Data analysis

Data are presented as means ± SEM. Statistical analyses were conducted using Prism 9 software (Graphpad Prism, RRID:SCR_002798) and significance was set at alpha < 0.05. Group comparisons were performed using analysis of variance (ANOVA; one-, two-, threeway) with Tukey or Sidak's post-hoc tests. Two-group comparisons used Student's t-tests. Specific analysis conducted are indicated in figure legends. Graphs were generated in Prism 9 software.

Results

Peri-AOF is associated with increased amyloid fibrils in select regions of the CA1 and CA3, but not in the dentate gyrus, in 5xFAD mice

AD dementia is more prevalent in women and may emerge at the onset of menopause. However, there is limited evidence that Aβ levels in the hippocampus, which are a hallmark of AD, are influenced by perimenopause. To evaluate whether Aβ increases in the hippocampus of females at a stage of early ovarian failure, 5xFAD females were treated with VCD, or sesame oil as a control, and Aβ levels quantified at peri-AOF, a stage corresponding to human perimenopause. To obtain a more granular understanding of perimenopause role on AD pathology, analysis was performed across major hippocampal subregions. Given the small size and complex geometric borders of these hippocampal subregions, ELISA and similar methods requiring precise tissue punches were not feasible. Instead, we employed light microscopic immunohistochemistry.

The density of 4G8, a marker of Aβ, was examined in CA1, CA3, DG and subicular subregions in rostral and caudal hippocampal sections of the 5xFAD mice (Figures 2A,B). No immunoreactivity was detected in the WT mice. As described below, 4G8 labeling in the 5xFAD mice varied across hippocampal subregions with sublayer specificity.

CA1 and subiculum: In the rostral CA1, dense 4G8-immunoreactivity (ir) was found in the pyramidal cell layer (PCL), with scattered clusters in the other laminae, particularly in the stratum oriens (SO) (Figure 2C–E). In the rostral CA1 PCL, 5xFAD male mice exhibited lower 4G8 labeling than both 5xFAD-oil treated and 5xFAD VCD-treated female mice following post-hoc analysis ($F = 5.080$, $p = 0.013$) (Figure 2F). Similarly, in the stratum radiatum (nSR), 5xFAD males showed lower 4G8 labeling compared to 5xFAD-oil treated female mice ($F = 3.783$, $p = 0.034$) (Figure 2F). Analogously, in the deep stratum radiatum (dSR), the density of 4G8 labeling following post-hoc analysis was lower in 5xFAD male mice compared to 5xFAD oil- and 5xFAD VCD-treated female mice ($F = 4.178$, $p = 0.025$) (Figure 2F). The 4G8 labeling in the caudal CA1 was similar to that seen rostrally. Moreover, scattered 4G8-positive cells were found in the subiculum though no significant effects were found (Supplementary Figures S1A–D).

CA3: Scattered 4G8-labeled cells were found in the PCL of CA3a and CA3b, with labeled clusters dispersed throughout other laminae (Figures 2G–I). No significant difference in 4G8 density was observed in any sublayers of CA3a (Supplementary Figures S1E–H). However, in the CA3b PCL, 5xFAD VCD females showed greater 4G8 labeling than both 5xFAD oil-treated females and 5xFAD male mice following *post hoc* analysis ($F = 5.049$, $p = 0.013$) (Figure 2J). Additionally, in the stratum lucidum (SLu) of CA3b, 5xFAD VCD-treated females showed higher 4G8 density than 5xFAD males ($F = 5.98$, $p = 0.007$; $t(20) = 3.374$, $p = 0.003$) (Figure 2J).

Dentate Gyrus (DG): In both the rostral and caudal DG, 4G8-labeling appeared in clusters throughout all laminae, especially in the hilus. No significant difference in 4G8 density was observed in any DG sublayers (Supplementary Figures S1I–P).

10.3389/fmolb.2025.1597130

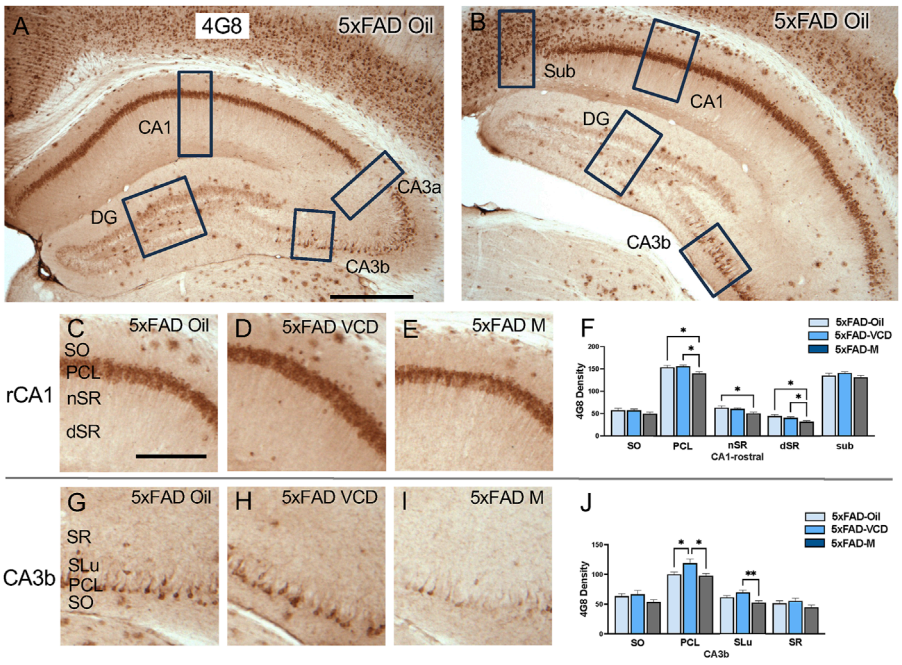

FIGURE 2
4G8 labeling is differentially altered in select regions of the hippocampus of oil and peri-AOF female and male 5xFAD mice. **(A,B)** Low-magnification photomicrographs of 4G8 labeling in the rostral **(A)** and caudal **(B)** hippocampus. Boxes indicate regions of the CA1, CA3a, CA3b, dentate gyrus (DG), and subiculum (Sub) that were sampled. **(C–E)** Representative photomicrographs showing 4G8 labeling in the rostral CA1 of 5xFAD-oil **(C)**, 5xFAD-VCD **(D)**, and 5xFAD-male mice **(E)**. **(F)** In the rostral CA1 PCL, and dSR, 5xFAD-male mice show significantly less 4G8 labeling than 5xFAD-oil and 5xFAD-VCD female mice. In the rostral CA1 nSR, 5xFAD-male mice show significantly less 4G8 labeling than 5xFAD-oil female mice. **(G–I)** Representative photomicrographs showing 4G8 labeling in the CA3b of 5xFAD-oil **(G)**, 5xFAD-VCD **(H)**, and 5xFAD-male mice **(I)**. **(J)** In the CA3b PCL, 5xFAD-VCD female mice show greater 4G8 labeling than both 5xFAD-oil female and 5xFAD-male mice. In the CA3b SLu, 5xFAD-VCD female mice show greater 4G8 labeling than 5xFAD-male mice.*p < 0.05;**p < 0.01 by One-way ANOVA with Tukey's post-hoc comparisons. Data are expressed as mean ± SEM, n = 11 animals per experimental group. Scale bars **(A,B)** = 500 μm, (C,D,E,G,H,I) = 200 μm.

Peri-AOF is associated with increased levels of reactive astrocytes in select regions of the rostral CA1,DG, and caudal CA1 of 5xFAD mice

Astrocytes facilitate the removal of Aβ from the brain parenchyma by mediating efflux into the cerebral vasculature (Liu et al., 2018). Their function is influenced by sex, partly through the actions of estrogen signaling via its estrogen receptors (Santos-Galindo et al., 2011; Chowen and Garcia-Segura, 2021; Lu et al., 2020). Therefore, astrocytes are expected to play an important role in amyloidosis during ovarian failure. However, evidence is limited regarding changes in astrocyte activity across hippocampal subregions in both intact and reproductively compromised females.

To assess astrocyte activation, the density of the astrocytic marker GFAP was examined in CA1, CA3, DG and subicular subregions within rostral and caudal hippocampus (Figures 3A,B) of WT and 5xFAD oil- and VCD-treated female mice, as well as oil-treated male mice. Consistent with our prior studies (Milner et al., 2022; Platholi et al., 2023), GFAP-labeled cells were found throughout all lamina of CA1, CA3 and DG, with fewer GFAP-positive cells in the pyramidal and granule cell layers (Figures 3,4,). Representative micrographs of GFAP labeling are shown for rostral CA1 (Figures 3C–H), caudal CA1/subiculum (Figures 3J–O), rostral DG (Figures 4A–F), and caudal DG (Figures 4H–M).

CA1 and subiculum: In the rostral CA1 SO region, there was a significant main effect of genotype ($F_{genotype}$ = 18.50, p < 0.0001) and treatment ($F_{treatment}$ = 3.770, p = 0.029). Post-hoc analysis showed that the density of GFAP labeling in SO was greater (p < 0.05) in 5xFAD mice than their WT counterparts (Figure 3I). In the PCL region, a significant main effect of treatment was found ($F_{treatment}$ = 4.822, p = 0.011),with WT-VCD mice showing greater GFAP labeling than WT male mice (p = 0.048) (Figure 3I). In the SLM region, a significant main effect of genotype was observed ($F_{genotype}$ = 12.20, p = 0.0009), and post-hoc analysis showed that 5xFAD male mice had significantly greater GFAP labeling than WT male mice (p = 0.006) (Figure 3I).

In the caudal CA1 SO region, there was a significant main effect of genotype ($F_{genotype}$ = 38.26, p < 0.0001). Post-hoc analysis showed increased GFAP labeling in 5xFAD mice compared to WT controls (p < 0.05) (Figure 3P). In the PLC region, a main effect of genotype was also observed ($F_{genotype}$ = 7.458, p = 0.008). Post-hoc multiple comparisons showed that WT-VCD mice had greater GFAP labeling than WT-oil mice (p = 0.022) (Figure 3P). Additionally, 5xFAD-oil mice had significant higher GFAP labeling in the PLC than WT-oil mice (p = 0.001) (Figure 3P). In the SR region, of caudal CA1, a significant main effect of genotype was observed ($F_{genotype}$ = 9.803, p = 0.003), with increased GFAP labeling in 5xFAD-oil compared to WT-oil mice (p = 0.005) (Figure 3P). In the SLM region, there was a significant main effect of genotype ($F_{genotype}$ = 12.49, p = 0.001),

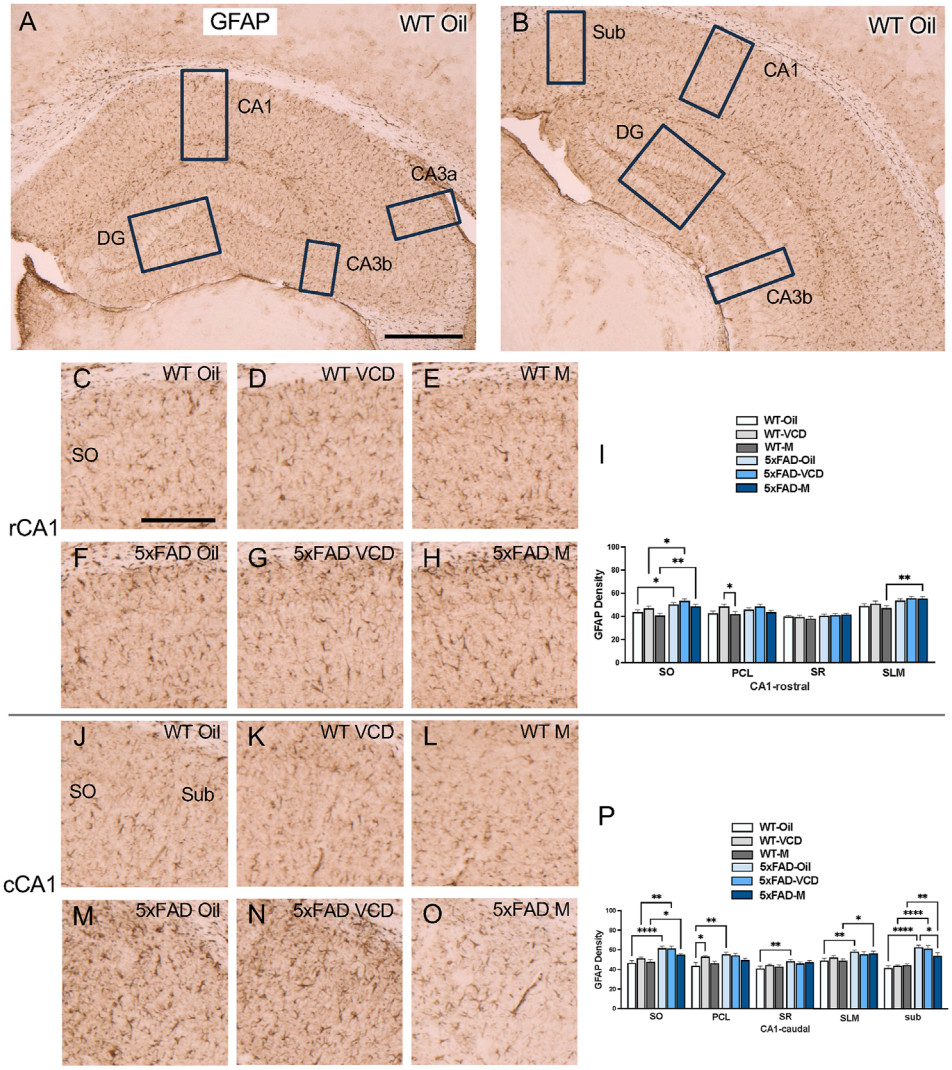

FIGURE 3
Increased GFAP labeling is associated with peri-AOF and/or 5xFAD genotype in select regions of the hippocampus. **(A,B)** Low-magnification photomicrographs of GFAP labeling in the rostral **(A)** and caudal **(B)** hippocampus. Boxes indicate regions of the CA1, CA3a, CA3b, dentate gyrus (DG), and subiculum (Sub) that were sampled. **(C–H)** Representative photomicrographs showing GFAP labeling in the rostral CA1 of WT-oil **(C)**, WT-VCD **(D)**, WT-male **(E)**, 5xFAD-oil **(F)**, 5xFAD-VCD **(G)**, and 5xFAD-male mice **(H)**. **(I)** In the rostral CA1 SO, the density of GFAP was increased in 5xFAD mice compared to WT mice, irrespective of sex/AOF treatment. In the PCL, WT-VCD female mice show greater GFAP density than WT-male mice. In the SLM, 5xFAD-male mice show more GFAP labeling than WT-male mice. **(J–O)** Representative photomicrographs showing GFAP labeling in the caudal CA1 of WT-oil **(J)**, WT-VCD **(K)**, WT-male **(L)**, 5xFAD-oil **(M)**, 5xFAD-VCD **(N)**, and 5xFAD-male mice **(O)**. **(P)** In the caudal CA1 SO, the density of GFAP was increased in 5xFAD mice compared to WT mice, irrespective of sex/AOF treatment. In the PCL WT-oil female mice show less GFAP labeling than 5xFAD-oil and WT-VCD female mice. In the SR, 5xFAD-oil female mice show greater GFAP density than WT-oil female mice. In the SLM, both 5xFAD-oil female and 5xFAD-male mice had greater GFAP labeling than WT-oil and WT-male mice, respectively. In the Sub, the density of GFAP was increased in 5xFAD mice compared to WT mice, irrespective of sex/AOF treatment, and 5xFAD-oil female mice showed greater GFAP labeling than 5xFAD-male mice.$^{*}p < 0.05;^{**}p < 0.01;^{****}p < 0.0001$ by two-way ANOVA with Tukey's hoc multiple comparison analysis. Data are expressed as mean ± SEM, n = 11 mice per experimental group. Scale bars **(A,B)** = 500 μm, (C,D,E,F,G,H,J,K,L,M,N,O) = 200 μm.

with 5xFAD-oil mice exhibiting greater GFAP labeling than WT-oil mice ($p = 0.0071$), and 5xFAD-male showing increased GFAP compared to WT-male mice ($p = 0.0243$) (Figure 3P). Similar to other regions of caudal CA1, in the subiculum, a significant main effect of genotype was found ($F_{genotype} = 61.46$, $p < 0.0001$), with post-hoc comparisons revealing greater GFAP labeling in 5xFAD mice compared to WT controls ($p < 0.05$) (Figure 3P). Additionally, 5xFAD-oil mice had significantly higher GFAP labeling in the subiculum than 5xFAD-male mice ($p = 0.045$) (Figure 3P).

CA3: No significant effect of treatment or genotype on GFAP density was observed in any CA3 subregions (Supplementary Figures S2A–N).

DG: In the rostral DG crest, there was a significant effect of genotype ($F_{genotype} = 6.914$, $p = 0.011$) on the density of GFAP labeling. Post-hoc analysis revealed significantly greater GFAP labeling in 5xFAD-VCD compared to WT-VCD mice ($p = 0.021$) (Figure 4G). In the hilus, a significant main effect of genotype was observed ($F_{genotype} = 12.21$, $p = 0.001$), with post-hoc multiple

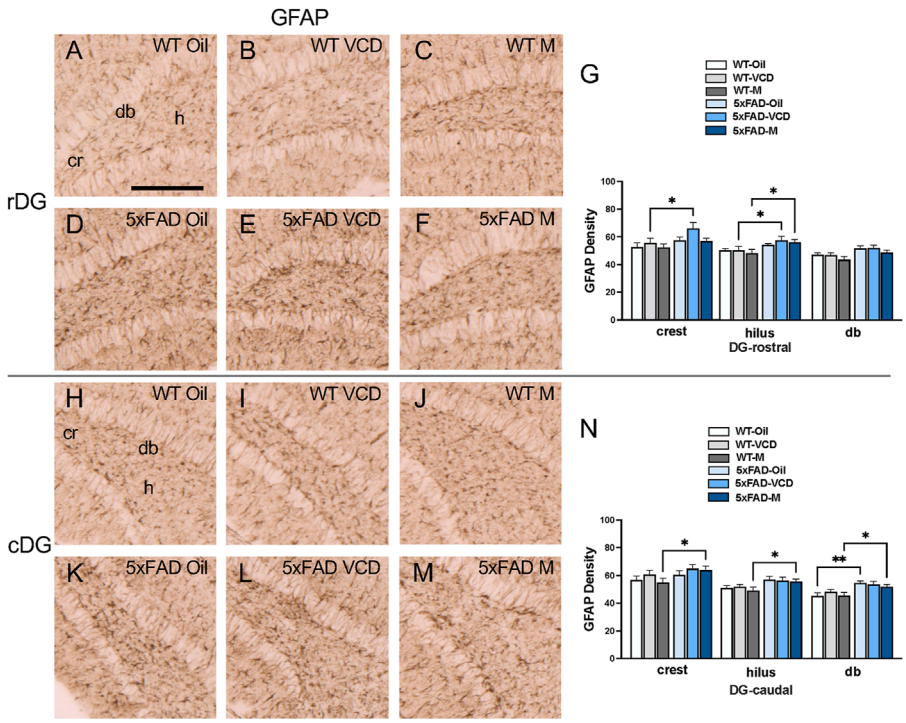

FIGURE 4
Increased GFAP labeling is associated with peri-AOF and/or 5xFAD genotype in select regions of the hippocampus. **(A–F)** Representative photomicrographs showing GFAP labeling in the rostral DG of WT-oil **(A)**, WT-VCD **(B)**, WT-male **(C)**, 5xFAD-oil **(D)**, 5xFAD-VCD **(E)**, and 5xFAD-male mice **(F)**. **(G)** In the rostral DG crest, 5xFAD-VCD female mice show increased GFAP labeling compared to WT-VCD female mice. In the hilus, 5xFAD-VCD female and 5xFAD-male mice show more GFAP labeling than WT-VCD female and WT-male mice, respectively. **(H–M)** Representative photomicrographs showing GFAP labeling in the caudal DG of WT-oil **(H)**, WT-VCD **(I)**, WT-male **(J)**, 5xFAD-oil **(K)**, 5xFAD-VCD **(L)**, and 5xFAD-male mice **(M)**. **(N)** In the caudal DG crest, hilus, and db, the density of GFAP was increased in 5xFAD-male mice compared to WT-male mice. In the db, GFAP density was also higher in 5xFAD-oil female mice compared to WT-oil female mice.*$p < 0.05$;**$p < 0.01$ by two-way ANOVA with Tukey's *post hoc* multiple comparison analysis. Data are expressed as mean ± SEM, n = 11 animals per experimental group. Scale bar = 200 μm.

comparison analysis revealing that 5xFAD-VCD and 5xFAD-male mice had greater GFAP labeling than their WT counterparts ($p < 0.05$) (Figure 4G).

In the caudal DG crest, there was a significant main effect of genotype ($F_{genotype} = 5.325$, $p = 0.025$), with increased GFAP in 5xFAD-male compared to WT-male mice ($p = 0.034$) (Figure 4N). In the hilus, a main effect of genotype was also found ($F_{genotype} = 10.18$, $p = 0.002$), with 5xFAD-male mice exhibiting greater GFAP labeling than WT-male mice ($p = 0.036$) (Figure 4N). In the db region of the DG, a main effect of genotype was observed ($F_{genotype} = 18.47$, $p < 0.0001$), with increased GFAP labeling in 5xFAD-oil compared to WT-oi mice ($p = 0.002$) (Figure 4N). Similarly to the crest and hilus, 5xFAD-male mice showed significantly more GFAP labeling than WT-male mice ($p = 0.031$) in the db (Figure 4N).

These patterns of GFAP labeling suggest that peri-AOF is associated with increased astrocyte activity in select hippocampal regions of the rostral and caudal CA1 and DG.

Increased microglia activation in select regions of the CA1 and DG of 5xFAD mice

Microglia, the brain's resident macrophage, regulate neuroinflammation and cognitive function (Cornell et al., 2022). The protein Iba1 is constitutively expressed in microglia and upregulated upon activation (Sasaki et al., 2001; Imai et al., 1996), a common feature of aging and neurodegenerative disorders (Prinz et al., 2021). Significantly, microglia activity is influenced by ovarian hormone changes. Ovariectomy increases Iba1 expression in middle-aged female mice (Sárvári et al., 2017), while estradiol reduces microglia reactivity in the hippocampus of aged ovariectomized animals (Lei et al., 2003). Additionally, ovariectomy elevates macrophage antigen complex-1, another marker of reactive microglia, in the hippocampus of aged mice (Benedusi et al., 2012). In AD mouse models, chronic estrogen deficiency is linked to heightened microglial activation and neurodegeneration (Prat et al., 2011). Given these findings, ovarian failure may alter hippocampal Iba1 expression during amyloidosis, however, direct evidence remains limited.

The density of Iba1 was examined in CA1, CA3, DG and subiculum subregions within the rostral and caudal hippocampus (Figures 5A,B). Consistent with our prior studies (Milner et al., 2022; Platholi et al., 2023), Iba1-labeled cells were scattered throughout all lamina in the CA1, CA3 and DG; however, the pyramidal and granule cell layers contained less Iba1 labeling (Figures 5,6,). Representative micrographs show the distribution of Iba1 labeling in the rostral CA1 (Figures 5C–H), caudal CA1/subiculum (Figures 5J–O), rostral DG (Figures 6A–F), and caudal DG (Fiures 6H–M).

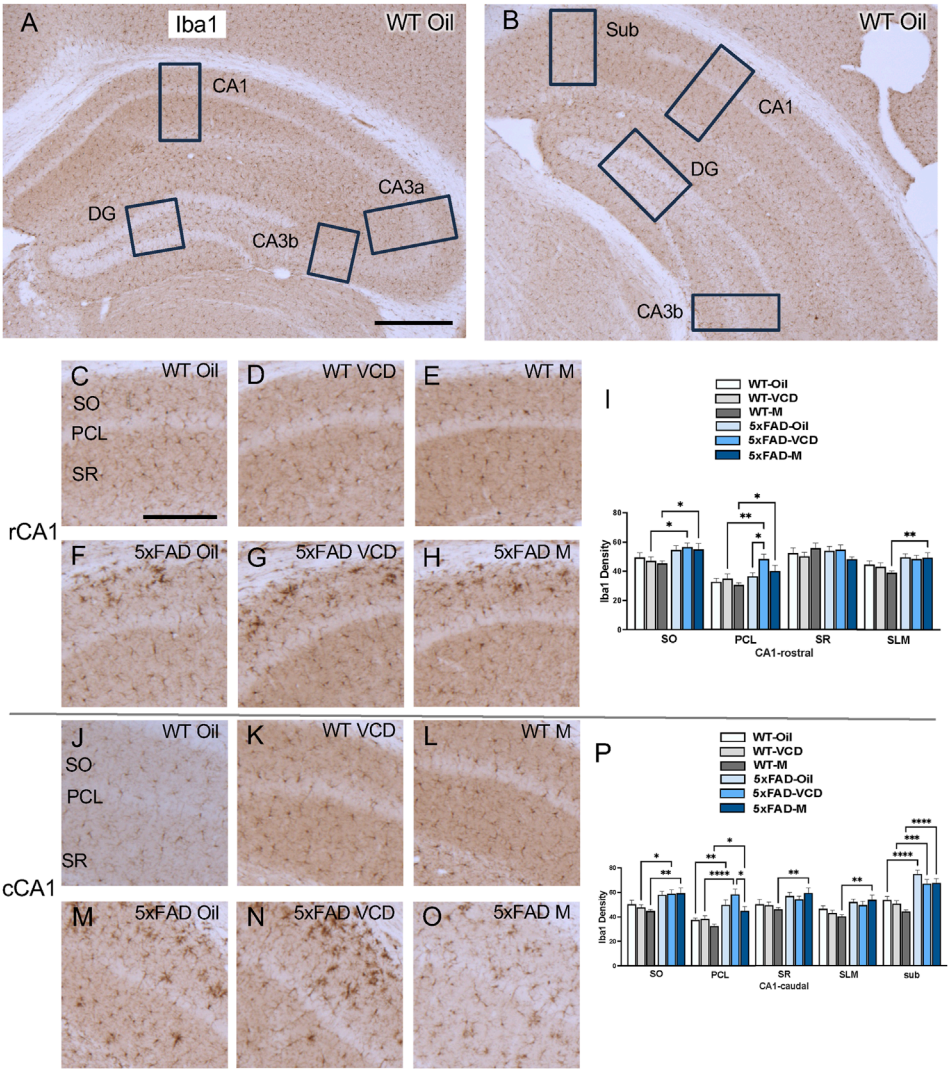

FIGURE 5
Increased Iba1 labeling is associated with peri-AOF and/or 5xFAD genotype in select regions of the hippocampus. **(A,B)** Low-magnification photomicrographs of Iba1 labeling in the rostral **(A)** and caudal **(B)** hippocampus. Boxes indicate regions of the CA1, CA3a, CA3b, dentate gyrus (DG), and subiculum (Sub) that were sampled. **(C–H)** Representative photomicrographs showing Iba1 labeling in the rostral CA1 of WT-oil **(C)**, WT-VCD **(D)**, WT-male **(E)**, 5xFAD-oil **(F)**, 5xFAD-VCD **(G)**, and 5xFAD-male mice **(H)**. **(I)** In the rostral CA1 SO and PCL, the density of Iba1 was increased in 5xFAD-VCD female and 5xFAD-male mice compared to WT-VCD female and WT-male mice, respectively. In the PCL, Iba1 density was greater in 5xFAD-VCD female mice than 5xFAD-oil female mice. In the SLM, 5xFAD-male mice had more Iba1 labeling than WT-male mice. **(J–O)** Representative photomicrographs showing Iba1 labeling in the caudal CA1 of WT-oil **(J)**, WT-VCD **(K)**, WT-male **(L)**, 5xFAD-oil **(M)**, 5xFAD-VCD **(N)**, and 5xFAD-male mice **(O)**. **(P)** In the caudal CA1 SO, 5xFAD-VCD female and 5xFAD-male mice had increased Iba1 density compared to WT-VCD and WT-male mice, respectively. In the PCL, the density of Iba1 was increased in 5xFAD mice compared to WT mice irrespective of sex/AOF treatment. 5xFAD-VCD female mice also showed greater Iba1 labeling than 5xFAD-male mice. In the SR and SLM, 5xFAD-male mice had more Iba1 labeling than WT-male mice. In the Sub, 5xFAD mice had increased Iba1 density compared to WT mice irrespective of sex/AOF treatment.*p < 0.05;**p < 0.01;***p < 0.001;****p < 0.0001 by two-way ANOVA with Tukey's *post hoc* multiple comparison analysis. Data are expressed as mean ± SEM, n = 11 animals per experimental group. Scale bars **(A,B)** = 500 μm, **(C,D,E,F,G,H,J,K,L,M,N,O)** = 200 μm.

CA1 and subiculum: In the rostral CA1 SO region, there was a significant main effect of genotype ($F_{genotype}$ = 10.16, p = 0.0023) on Iba1 labeling. Post-hoc analysis showed that Iba1 density was greater (p < 0.05) in 5xFAD-VCD and 5xFAD-male than their WT counterparts (Figure 5I). In the PCL region, there was a main effect of genotype ($F_{genotype}$ = 14.12, p = 0.0004) and treatment ($F_{treatment}$ = 3.449, p = 0.038) on Iba1 labeling. As in the SO region, post-hoc analysis showed increased labeling in 5xFAD-VCD and 5xFAD-male mice (p < 0.05) compared to WT mice (Figure 5I). Additionally, 5xFAD-VCD mice exhibited significantly more Iba1 labeling compared to 5xFAD-oil, mice (p = 0.016) (Figure 5I). In the SLM region of the rostral CA1, a main effect of genotype was observed ($F_{genotype}$ = 10.89, p = 0.002), with post-hoc analysis showing significantly more Iba1 labeling in 5xFAD-male mice than WT-male mice (p = 0.006) (Figure 5I).

In the caudal CA1 SO region, there was a significant main effect of genotype ($F_{genotype}$ = 19.61, p < 0.0001). Post-hoc analysis showed that Iba1 density was greater (p < 0.05) in 5xFAD-VCD and 5xFAD-male

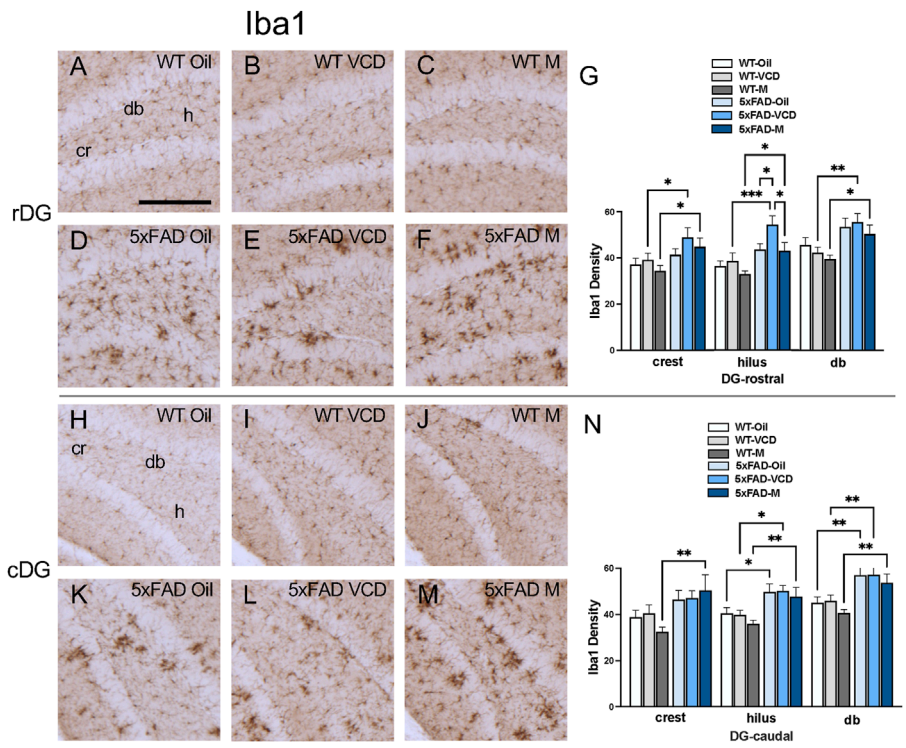

FIGURE 6
Increased Iba1 labeling is associated with peri-AOF and/or 5xFAD genotype in select regions of the hippocampus. **(A–F)** Representative photomicrographs showing Iba1 labeling in the rostral DG of WT-oil **(A)**, WT-VCD **(B)**, WT-male **(C)**, 5xFAD-oil **(D)**, 5xFAD-VCD **(E)**, and 5xFAD-male mice **(F)**. **(G)** In the rostral DG crest and db, 5xFAD-VCD female and 5xFAD-male mice showed greater Iba1 labeling than WT-VCD and WT-male mice, respectively. In the hilus, the density of Iba1 labeling was increased in 5xFAD mice compared to WT mice, irrespective of sex/AOF treatment. 5xFAD-VCD female mice also showed greater Iba1 labeling than 5xFAD-male mice. **(H–M)** Representative photomicrographs showing GFAP labeling in the caudal DG of WT-oil **(H)**, WT-VCD **(I)**, WT-male **(J)**, 5xFAD-oil **(K)**, 5xFAD-VCD **(L)**, and 5xFAD-male mice **(M)**. **(N)** In the caudal DG crest, 5xFAD-male mice had greater Iba1 labeling than WT-male mice. In the hilus and db, the density of Iba1 was increased in 5xFAD mice compared to WT mice, irrespective of sex/AOF treatment.*p < 0.05;**p < 0.01;***p < 0.001;****p < 0.0001 by two-way ANOVA with Tukey's *post hoc* multiple comparison analysis. Data are expressed as mean ± SEM, n = 11 animals per experimental group. Scale bar = 200 μm.

mice than their WT counterparts (Figure 5P). In the PCL region, a main effect of genotype ($F_{genotype}$ = 30.99, p < 0.0001) and treatment ($F_{treatment}$ = 4.272, p = 0.014) was observed. Multiple comparisons revealed significantly more Iba1 labeling in 5xFAD mice than in WT mice (p < 0.05) (Figure 5P). Additionally, 5xFAD-VCD mice exhibited greater Iba1 labeling in the PLC than 5xFAD-male mice, (p = 0.014) (Figure 5P). In the SR region of the caudal CA1, a main effect of genotype ($F_{genotype}$ = 9.983, p = 0.003) was found, with post-hoc analysis showing significantly more Iba1 in 5xFAD-male mice than in WT-male mice (Figure 5P). In the SLM, there was also a main effect of genotype ($F_{genotype}$ = 14.19, p = 0.0004), with 5xFAD-male mice exhibiting greater Iba1 labeling than WT-male mice (Figure 5P). Similarly, in the subiculum, a significant main effect of genotype ($F_{genotype}$ = 67.47, p < 0.0001) and treatment ($F_{treatment}$ = 3.996, p = 0.024) was found, with post-hoc analysis revealing significantly more Iba1 labeling in 5xFAD mice than WT mice (p < 0.05) (Figure 5P).

CA3: There was no effect of treatment or genotype on the density of Iba1 labeling in any of the sublayers of CA3a or CA3b (Supplementary Figures S2O–AB).

DG: In the rostral DG, there was a significant main effect of genotype ($F_{genotype}$ = 9.923, p = 0.0025) on Iba1 labeling in the crest. Post-hoc analysis showed greater Iba1 density (p < 0.05) in 5xFAD-VCD and 5xFAD-male mice than in WT mice (Figure 6G). In the hilus, there was a main effect of genotype ($F_{genotype}$ = 20.20, p < 0.0001) and treatment ($F_{treatment}$ = 4.349, p = 0.017). Post-hoc analysis showed significantly more Iba1 labeling (p < 0.05) in 5xFAD-VCD and 5xFAD-male mice compared to their WT counterparts (Figure 6G). Additionally, 5xFAD-VCD mice exhibited increased Iba1 density compared to 5xFAD-oil mice (p = 0.036) and 5xFAD-male mice (p = 0.027) (Figure 6G). In the db of the rostral DG, a main effect of genotype ($F_{genptype}$ = 16.39, p = 0.0002) was observed, with post-hoc analysis showing greater density of Iba1 (p < 0.05) in 5xFAD-VCD and 5xFAD-male mice compared to WT mice (Figure 6G).

In the caudal DG, a main effect of genotype ($F_{genotype}$ = 10.04, p = 0.002) was found in the crest, with 5xFAD males exhibiting greater Iba1 density than WT male mice (p = 0.003) (Figure 6N). In the caudal hilus, a significant main effect of genotype ($F_{genotype}$ = 20.42, p < 0.0001) was observed, with post-hoc analysis showing greater Iba1 labeling (p < 0.05) in 5xFAD mice than in their WT counterparts (Figure 6N). Similarly, a significant main effect of genotype ($F_{genotype}$ = 25.07, p < 0.0001) was determined in the db of the DG, with multiple comparisons revealing significantly more Iba1-labeling (p < 0.01) in 5xFAD mice than in WT mice (Figure 6N).

These results suggest that the 5xFAD genotype at peri-AOF influences microglia activation in multiple subregions of rostral and caudal CA1and DG compared to peri-AOF WT mice. Additionally, peri-AOF further exacerbates microglia activation in 5xFAD mice in rostral CA1 PCL and DG hilus, suggesting sex-dependent vulnerability. These findings, in concert with increased GFAP labeling in select hippocampal regions, suggest enhanced susceptibility to neuroinflammation at the intersection of AD and perimenopause.

Cognitive impairment varies with genotype, sex and AOF

Neuroinflammation is intrinsically linked to the progression of cognitive impairment and dementia (Heneka et al., 2015). However, the impact of early ovarian failure on cognitive function in VCD-treated 5xFAD mice, and how this compares to males, remains unknown. To address this, we assessed the behavioral consequences of early ovarian decline in 5xFAD mice compared to non-VCD treated females and males using different cognitive tests sensitive to Aβ pathology, including the Y-maze alternation test, novel object recognition, and spatial navigation in the Barnes maze.

Y-maze

No significant differences were observed in arm alternation behavior (Figure 7A) or in the total number of arm entries in all 3 arms during the testing period (Figure 7B) between 5xFAD and WT mice. No differences were observed in the % novel arm entries respect to total arm entries and in the time spent in the novel arm (data not shown). This may suggest preservation of short-term working memory or that other cognitive domains might be more affected in 5xFAD mice and in VCD-treated females at a young age.

Novel object

An effect of AOF was seen in locomotor activity as assessed by total distance travelled ($F(5, 60) = 2.42$, $p = 0.05$). 5xFAD-male compared to 5xFAD-VCD female mice had a lower total distance ($p = 0.06$), although not significant (Figure 7C). No significant differences across groups were observed in the total object exploration time or in Novel Object Recognition Index (Figures 7D,E). Interestingly, significant increase in time spent exploring the novel object vs. the familiar object was observed between WT-male ($p < 0.0001$) and 5xFAD-male mice ($p = 0.001$) (Figure 7F). For females, significant differences in time spent exploring familiar and novel objects were found between treatment in WT mice (WT-female ($p = 0.018$); WT-VCD female ($p = 0.014$)), but did not extend to 5xFAD females (Figure 7F).

Barnes maze

There were no significant differences in motor activity, as assessed by distance traveled and mean speed between 5xFAD and WT mice, regardless of genotype or treatment (Figures 8A,B). Although, a significance difference was observed in mean speed between WT females and VCD-treated WT females at day 1 only ($p = 0.0086$). Also, no differences were observed in learning measures as shown for latency to find the escape and path efficiency (Figures 8C,D).

When cognitive performance was tested 24 h after the final acquisition training session, VCD-treated WT-females spent significantly less time in the target quadrant where the escape hole was located, and more time in non-target quadrants compared to both WT-oil or 5xFAD-VCD females (Figures 8E,F).

Given that the Barnes maze is a measure of spatial learning and memory, the altered performance in VCD-treated WT females suggests a potential adverse effect of early ovarian failure on spatial memory. This effect appears to be mitigated in 5xFAD-VCD females.

Overall, these behavioral data demonstrate that VCD treatment impairs performance in select cognitive tasks. Combined with our anatomical findings on Aβ deposition and glia activation in the hippocampus, these results suggest that early ovarian failure contributes to early-stage AD-like neurobehavioral pathology.

Discussion

The relationship between early ovarian failure and neuroinflammation in the hippocampus was investigated using a model of perimenopausal AD that combined chemically-induced AOF with transgenic 5xFAD mice. Age-matched males were also tested in tandem. Mice at approximately 4-months of age showed complex effects on production of Aβ as well as signs of astrocyte and microglia activity that varied by genotype, VCD treatment (AOF) and sex. We found that Aβ expression was elevated in female 5xFAD mice, but only further increased in peri-AOF mice in select hippocampal subregions. Further, increases in glial activation also paralleled Aβ pathology but only in discrete areas of the hippocampus. Assessment of cognitive function showed no effect of peri-AOF in the Y-maze, in the Novel Object Recognition tests, or across Barnes Maze training days (days 1–4). Interestingly, peri-AOF reduced the time spent in the Barnes Maze target quadrant during the testing day (day 5) in WT but not in 5xFAD females, suggesting a treatment-genotype interaction effect. These data provide preclinical experimental evidence supporting the contention that peri-menopause is a sensitive period for neuroinflammation and cognitive function in women.

AD, the most prevalent of the dementias (Alzheimer's, 2016), is classically characterized by Aβ deposition and cognitive impairment. However, AD also involves a complex set of neurodegenerative processes, including neuroinflammation (Lista et al., 2024). Importantly, the incidence, progression, and severity of the disease are greater in women (Pike, 2017; Laws et al., 2016). Further, perimenopause may be a critical period for the emergence of AD, suggesting that altered gonadal hormone levels contribute to the increased AD risk (Gong et al., 2022). Although perimenopause represents a potential turning point in AD pathology, the impact of associated hormonal changes on hippocampal pathology remains unclear. To investigate the role of early ovarian decline in AD pathology, we exposed female 5xFAD mice to the ovotoxin VCD to induce AOF and tested them at an

10.3389/fmolb.2025.1597130

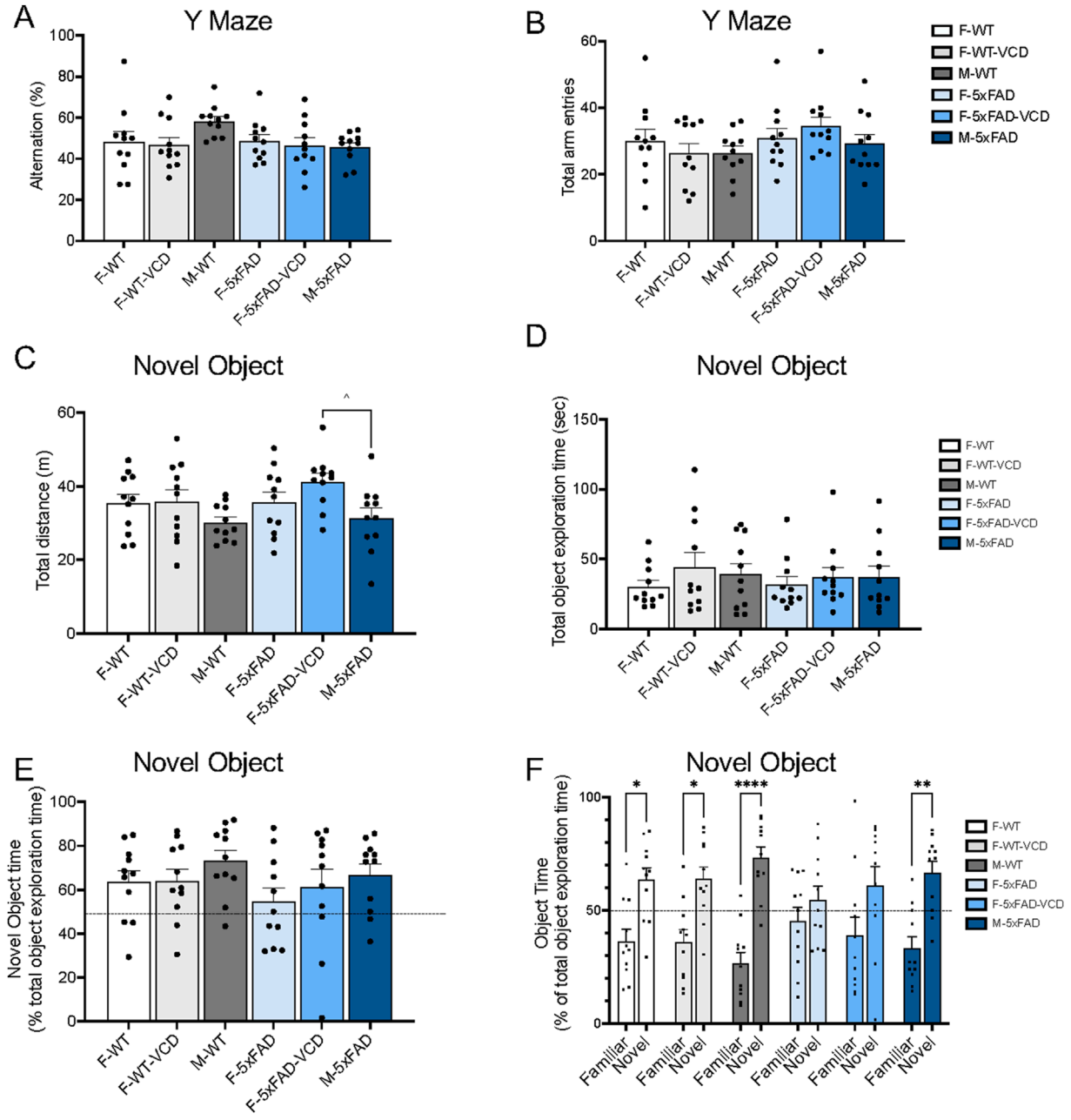

FIGURE 7
Cognition is not impaired in the Y-maze but is in the novel object recognition test in 5xFAD compared to WT mice. **(A,B)** In the Y-maze test, there were no significant differences in arm alternation behavior **(A)** or in the number of arm entries **(B)** between 5xFAD and WT mice. **(C)** Spontaneous motor activity tended to be decreased in 5xFAD-male mice compared to 5xFAD-VCD female mice. **(D)** total object exploratory time was not changed across experimental groups. **(E)** No significant differences were observed between groups in the percentage time spent exploring the novel object. **(F)** Significant increase in time spent with the novel object vs familiar object was observed for WT male and female (oil and VCD), as well as in 5xFAD male mice. This difference is lost in 5xFAD females. ^$p = 0.06$;*$p < 0.05$;**$p < 0.01$;****$p < 0.0001$ by one-way ANOVA with Sidak's *post hoc* multiple comparison analysis. Data are expressed as mean ± SEM, n = 11 animals per experimental group.

age when brain amyloid deposition and ovarian failure are both at early stages. Age-matched WT mice and 5xFAD male mice were also studied to isolate the impact of AOF independently of amyloidosis and to characterize sex differences, respectively.

We found that Aβ expression was elevated in female 5xFAD peri-AOF mice (injected with VCD) compared to intact females and males injected with sesame oil, in select hippocampal subregions such as the CA1 and CA3b, but not CA3a. The mechanism underlying increased Aß levels in CA3b compared to CA3a in VCD-treated 5xFAD mice is unclear at present. Presumably, these regional differences are mediated by neurophysiological (Hemond et al., 2009; Wittner and Miles, 2007), transcriptional (Cembrowski et al., 2016; Thompson et al., 2008), connectional (Wu et al., 1998), morphological (Wittner and Miles, 2007) and

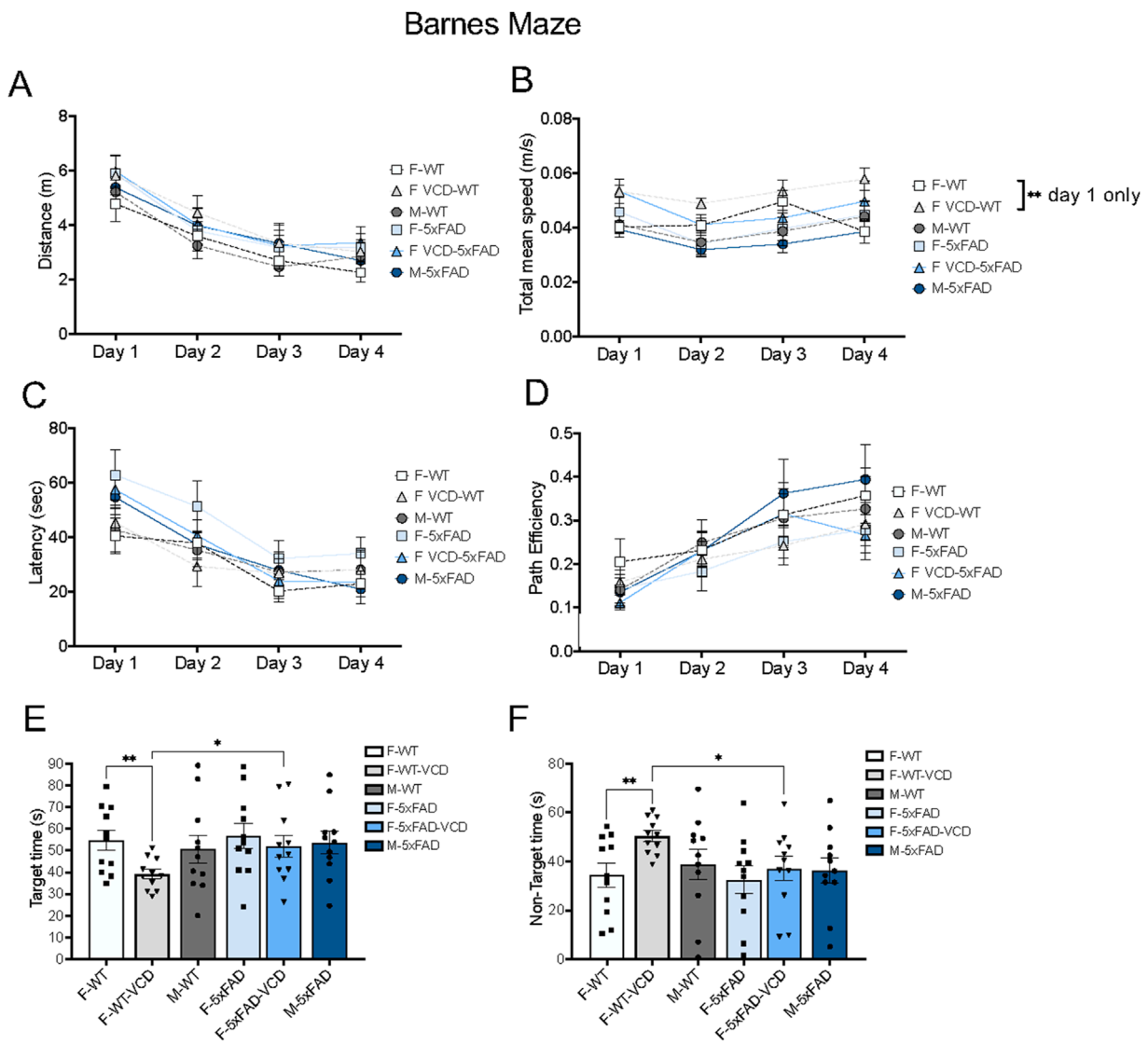

FIGURE 8
Cognitive performance is differentially affected on the Barnes maze test in peri-AOF female mice. **(A–D)** There were no observed differences in motor activity **(A,B)** and learning performance **(C,D)** in 5xFAD mice compared to WT mice over time by 2way ANOVA. **(E,F)** WT-VCD female mice demonstrated memory deficits compared to WT-oil and 5xFAD-VCD female mice.*$p < 0.05$;**$p < 0.01$ by 2way ANOVA with Tukey's post-hoc comparison analysis **(A–D)** or student's unpaired t-test **(E,F)**. Data are expressed as mean ± SEM, $N = 11$ animals per experimental group.

functional (Sun et al., 2017) divergence across these CA3 subfields, which in turn may be modulated by sex and estrogens. For example, CA3b and CA3a each show unique changes in expression patterns of both stress and plasticity-related molecules following stress, a modulator of dementia (Yakemow et al., 2024), and do so in an estrogen-dependent manner (Van Kempen et al., 2014; Pierce et al., 2014; Van Kempen et al., 2013). These results suggest that the pathways linking Aß pathology with estrogen signaling within the CA3 are subregion-specific, and further research is needed to clarify their specific contributions to learning and memory during ovarian failure.

In VCD-injected WT mice, GFAP density was increased compared to oil-treated WT mice in the caudal CA1 PCL and compared to males in the rostral CA1 PCL. No differences were detected with regard to Iba-1 labeling in any hippocampal region between the WT mice. The increased astrogliosis observed during peri-AOF may result from the loss of astrocyte estrogen signaling. Both resting and activated astrocytes are prominent among the non-neuronal hippocampal cell types that express estrogen receptors alpha and beta (Mitterling et al., 2010; Azcoitia et al., 1999; Sakuma et al., 2009) as well as G-protein estrogen receptors (Waters et al., 2015). Further, the expression and cellular location of estrogen receptors in the hippocampus are influenced by estrogen levels (Rune et al., 2002; Adams et al., 2002). Estrogen modulates GFAP expression (Stone et al., 1998) and regulates the expression of genes involved in astrocyte proliferation (Ma et al., 2014). Importantly, the CA1 PCL is an estrogen receptor-expressing region of the hippocampus (Mitterling et al.,

2010; Azcoitia et al., 1999; Sakuma et al., 2009) and is a major hippocampal output that plays a critical role in both spatial and non-spatial memory processes (Cinalli et al., 2023). The functional impact of elevated astrocyte activation in the context of reduced estrogen signaling remains unclear, although it may involve the loss of estrogen-mediated neuroprotection and/or the activation of compensatory mechanisms. This is supported by findings that estrogen reduces glucose- and oxygen-deprivation-induced apoptosis in astrocyte-neuron co-cultures, and that estrogen replacement attenuates the increased apoptosis in the CA1 produced by cerebral ischemia (Ma et al., 2016). Given the protective role of estrogen against astrocytosis-associated neural dysfunction, its loss in the CA1 PCL region suggests an increased vulnerability to stress or insult and a heightened propensity for neural pathology.

In addition to their critical metabolic role, astrocytes exert important effects on neuronal signaling and plasticity, particularly via modulation of pyramidal cells (Bosson et al., 2017; Dong et al., 2020). CA1 pyramidal cell hyperexcitability is a hallmark of neurodegeneration and, in particular, is observed in AD models (Šišková et al., 2014; Phelan et al., 2024; Lei et al., 2012). Significantly, astrocytes contribute to CA1 pyramidal cell activity (Courtney et al., 2023; Bohmbach et al., 2022; Wang et al., 2021), and reactive astrocytes are associated with decreased inhibitory synaptic currents and CA1 hyperexcitability (Ortinski et al., 2010). Thus, increased astrocyte activity in the CA1 PCL during early AOF, in the context of disrupted estrogen signaling, may contribute to conditions favoring pyramidal cell dysfunction.

We examined astrogliosis and Aβ expression in peri-AOF 5xFAD mice. Compared to WT VCD-treated mice, 5xFAD VCD mice did not show a further increase in GFAP in the CA1 PCL. However, GFAP density was increased in the CA1 SO and subiculum in VCD-treated 5xFAD mice compared to similarly treated WT mice. Additionally, 5xFAD peri-AOF mice showed higher GFAP density in the crest and hilus of the rostral DG compared to WT mice.

Microglia activation was also observed. Iba-1 levels were higher in peri-AOF 5xFAD mice compared to peri-AOF WT mice in the CA1 PCL, SO and subiculum as well as the different subregions of the DG These results indicate that microglia are recruited in non-pyramidal cell regions of the CA1. Significantly, microglia activation was greater in CA1 PCL and DG hilus cells in 5xFAD peri-AOF mice compared to 5xFAD females and males.

The increased 4G8 density observed in 5xFAD mice was expected to be coupled with elevated GFAP and Iba-1 levels. We found that in VCD-treated mice only the CA3b PCL showed increased Aβ compared to both oil-treated female and male controls. However, there were no differences in either GFAP or Iba-1 across any treatment in any CA3 field. Additionally, in both oil and VCD 5xFAD mice, 4G8 in the CA1 PCL was higher compared to males. Yet, this was associated with increased Iba-1 only in peri-AOF mice, suggesting that this region may be particularly sensitive in response to AOF and Aβ aggregation. The lack of coupling between increased neuroinflammatory markers and Aβ levels in several hippocampal subregions suggests that peri-AOF affects glial activity independently of amyloid aggregation in these areas. Alterations in brain function have been described prior to Aβ plaque or fibril formation in other APP overexpressing mouse models (Park et al., 2004). For example, functional hyperemia is impaired in young mice prior to Aβ aggregation (Park et al., 2004) and deficits in autoregulation occur (Niwa et al., 2002). These effects may be attributed to the actions of soluble oligomeric Aβ (Tolar et al., 2021), which are detectable in 5xFAD mice at the age range studied here (Habashi et al., 2022). Notably, oligomeric Aβ can impact astrocytes (Matafora et al., 2023) and microglia (Tong et al., 2024).

Our findings in 5xFAD mice contrast with similar experiments in SwDI mice, a model of cerebral amyloid angiopathy (Xu et al., 2014a; Xu et al., 2007). In SwDI VCD mice, we found increased 4G8 in the CA1 SO and DG. Further, astrocyte and microglia activation was observed in the CA1 SO, and astrocytes in the DG crest. Pyramidal cell layers of the CA1 and CA3 were not affected. These results indicate that dementia models with Aβ pathology in either parenchyma or cerebral vasculature exhibit distinct patterns of hippocampal amyloid deposition and glial cell activation with notable differences in pyramidal and non-pyramidal regions.

The present results demonstrate that distinct hippocampus regions exhibit differential susceptibility to AOF and Aβ in 5xFAD mice. The CA1 of 5xFAD mice, particularly the pyramidal cell layer, was vulnerable to the neuroinflammatory effects of peri-AOF. This aligns with evidence that the CA1 is the earliest hippocampal subregion to exhibit neuronal loss in AD (Padurariu et al., 2012; Kerchner et al., 2012) and that astrocyte-pyramidal cell interactions in the CA1 are disrupted in AD models (Pirttimaki et al., 2013).

Interestingly, the pyramidal cell layer of the CA3b region uniquely demonstrated elevated Aβ in 5xFAD peri-AOF mice. The CA3 is a region that expresses estrogen receptors (Mitterling et al., 2010; Mitra et al., 2003; Weiland et al., 1997; Shughrue and Merchenthaler, 2000; Tsurugizawa et al., 2005), contains estrogen-sensitive neurons (Van Kempen et al., 2014), and may be protected against Aβ-mediated degeneration by estrogen (Pike, 1999). Together with our findings in WT mice, these results suggest that pyramidal cell layers of the CA1 and CA3 fields are particularly sensitive to decreased estrogen and increased Aβ during early AOF in female mice. In sum, these findings highlight the complex interplay between ovarian hormone loss, neuroinflammation, and amyloid pathology, underscoring the need for further research into the mechanisms by which perimenopause contributes to heightened AD susceptibility in women.

Data availability statement

The original contributions presented in the study are included in the article/Supplementary Material, further inquiries can be directed to the corresponding authors.

Ethics statement

The animal study was approved by Weill Cornell Medicine Institutional Animal Care and Use Committees. The study was conducted in accordance with the local legislation and institutional requirements.

Author contributions

RM: Formal Analysis, Investigation, Methodology, Visualization, Writing – original draft, Writing – review and editing. JP: Formal Analysis, Investigation, Methodology, Visualization, Writing – original draft, Writing – review and editing. LP: Formal Analysis, Methodology, Supervision, Writing – review and editing, Writing – original draft. FY: Data curation, Investigation, Methodology, Writing – original draft, Writing – review and editing. GS: Data curation, Investigation, Visualization, Writing – original draft, Writing – review and editing, Formal Analysis. CW: Writing – original draft, Writing – review and editing. TM: Methodology, Supervision, Project administration, Conceptualization, Writing – original draft, Funding acquisition, Validation, Visualization, Resources, Writing – review and editing, Investigation. MG: Supervision, Conceptualization, Funding acquisition, Software, Investigation, Writing – review and editing, Visualization, Project administration, Writing – original draft, Validation, Resources, Data curation.

Funding

The author(s) declare that financial support was received for the research and/or publication of this article. Work was supported by NIH grants R01 HL136520S1 (TM and MG) and HL135498 (MG), R01 HL135428 (MG), R01 GM130722 (JP), R21 AG064455 (RM), R01 NS097805 (LP).

Conflict of interest

The authors declare that the research was conducted in the absence of any commercial or financial relationships that could be construed as a potential conflict of interest.

Correction note

A correction has been made to this article. Details can be found at: 10.3389/fmolb.2025.1684511.

Generative AI statement

The author(s) declare that no Gen AI was used in the creation of this manuscript.

Publisher's note

Supplementary material

The Supplementary Material for this article can be found online at: https://www.frontiersin.org/articles/10.3389/fmolb.2025.1597130/full#supplementary-material

SUPPLEMENTARY FIGURE S1
4G8 labeling is not altered in select regions of the hippocampus of across WT and 5xFAD experimental groups. **(A–C)**. Representative photomicrographs showing 4G8 labeling in the caudal CA1 of 5xFAD-oil **(A)**, 5xFAD-VCD **(B)**, and 5xFAD-male mice **(C)**. **(D)** In the caudal CA1, there were no significant differences in 4G8 labeling between 5xFAD-oil, 5xFAD-VCD female, and 5xFAD-male mice. **(E–G)** Representative photomicrographs showing 4G8 labeling in the rostral CA3a of 5xFAD-oil **(E)**, 5xFAD-VCD **(F)**, and 5xFAD-male mice **(G)**. **(H)** In the CA3a, there were no significant differences in 4G8 labeling observed between 5xFAD-oil, 5xFAD-VCD female, and 5xFAD-male mice. **(I–K)** Representative photomicrographs showing 4G8 labeling in the rostral DG of 5xFAD-oil **(I)**, 5xFAD-VCD **(J)**, and 5xFAD-male mice **(K)**. L. In the rostral DG, there were no significant differences in 4G8 labeling observed between 5xFAD-oil, 5xFAD-VCD female, 5xFAD-male mice. **(M–O)** Representative photomicrographs showing 4G8 labeling in the caudal DG of 5xFAD-oil (M), 5xFAD-VCD **(N)**, and 5xFAD-male mice **(O)**. **(P)** In the caudal DG, there were no significant differences in 4G8 labeling between 5xFAD-oil, 5xFAD-VCD female, and 5xFAD-male mice. Statistics was calculated by One-way ANOVA with Tukey's post-hoc multi comparison analysis. Data are expressed as mean ± SEM, n = 11 mice/group. Scale bar = 200 μm.

SUPPLEMENTARY FIGURE S2
GFAP and Iba1 labeling is unchanged in the CA3a and CA3b regions of the hippocampus of WT and 5xFAD female and male mice. **(A–F)** Representative photomicrographs showing GFAP labeling in the rostral CA3a of WT-oil **(A)**, WT-VCD **(B)**, WT-male **(C)**, 5xFAD-oil **(D)**, 5xFAD-VCD **(E)**, and 5xFAD-male mice **(F)**. **(G)** In the CA3a, there were no significant differences in GFAP labeling across groups. **(H–M)**. Representative photomicrographs showing GFAP labeling in the rostral DG of WT-oil **(H)**, WT-VCD **(I)**, WT-male **(J)**, 5xFAD-oil **(K)**, 5xFAD-VCD **(L)**, and 5xFAD-male mice **(M)**. **(N)**. In the CA3b, there were no significant differences in GFAP labeling across groups. **(O–T)** Representative photomicrographs showing Iba1 labeling in the rostral DG of WT-oil **(O)**, WT-VCD **(P)**, WT-male **(Q)**, 5xFAD-oil **(R)**, 5xFAD-VCD **(S)**, and 5xFAD-male mice **(T)**. **(U)** In the CA3a, there were no significant differences in Iba1 labeling across groups. **(V–Z)**, (AA). Representative photomicrographs showing Iba1 labeling in the rostral DG of WT-oil **(V)**, WT-VCD **(W)**, WT-male **(X)**, 5xFAD-oil **(Y)**, 5xFAD-VCD **(Z)**, and 5xFAD-male mice (AA). (AB) In the CA3a, there were no significant differences in Iba1 labeling across groups. Statistics was calculated by two-way ANOVA with Tukey's *post hoc* multiple comparison analysis. Data are expressed as mean ± SEM, *n* = 11 animals per experimental group. Scale bar = 200 μm.

References

Abi-Ghanem, C., Kelly, R. D., Groom, E. A., Valerian, C. G., Paul, A. S., Thrasher, C. A., et al. (2025). Interactions between menopause and high-fat diet on cognition and pathology in a mouse model of Alzheimer's disease. *Alzheimers Dement.* 21 (3), e70026. doi:10.1002/alz.70026

Abi-Ghanem, C., Salinero, A. E., Smith, R. M., Kelly, R. D., Belanger, K. M., Richard, R. N., et al. (2024). Effects of menopause and high fat diet on metabolic outcomes in a mouse model of alzheimer's disease. *J. Alzheimers Dis.* 101 (4), 1177–1194. doi:10.3233/JAD-231332

Adams, M. M., Fink, S. E., Shah, R. A., Janssen, W. G. M., Hayashi, S., Milner, T. A., et al. (2002). Estrogen and aging affect the subcellular distribution of estrogen receptor-alpha in the hippocampus of female rats. *J. Neurosci.* 22 (9), 3608–3614. doi:10.1523/jneurosci.22-09-03608.2002

Alafuzoff, I., Thal, D. R., Arzberger, T., Bogdanovic, N., Al-Sarraj, S., Bodi, I., et al. (2009). Assessment of beta-amyloid deposits in human brain: a study of the BrainNet Europe Consortium. *Acta Neuropathol.* 117 (3), 309–320. doi:10.1007/s00401-009-0485-4

Alzheimer's, A. (2016). 2016 Alzheimer's disease facts and figures. *Alzheimers Dement.* 12, 459–509. doi:10.1016/j.jalz.2016.03.001

Alzheimer's disease facts and figures (2023). *Alzheimers Dement.* 19 (4), 1598–1695. doi:10.1002/alz.13016

Arvanitakis, Z., Shah, R. C., and Bennett, D. A. (2019). Diagnosis and management of dementia: review. *Jama* 322 (16), 1589–1599. doi:10.1001/jama.2019.4782

Azcoitia, I., Sierra, A., and Garcia-Segura, L. M. (1999). Localization of estrogen receptor beta-immunoreactivity in astrocytes of the adult rat brain. *Glia* 26 (3), 260–267. doi:10.1002/(sici)1098-1136(199905)26:3<260::aid-glia7>3.0.co;2-r

Benedusi, V., Meda, C., Della Torre, S., Monteleone, G., Vegeto, E., and Maggi, A. (2012). A lack of ovarian function increases neuroinflammation in aged mice. *Endocrinology* 153 (6), 2777–2788. doi:10.1210/en.2011-1925

Bhattacharya, S., Haertel, C., Maelicke, A., and Montag, D. (2014). Galantamine slows down plaque formation and behavioral decline in the 5XFAD mouse model of Alzheimer's disease. *PLoS One* 9 (2), e89454. doi:10.1371/journal.pone.0089454

Blackwell, J. A., Silva, J. F., Louis, E. M., Savu, A., Largent-Milnes, T. M., Brooks, H. L., et al. (2022). Cerebral arteriolar and neurovascular dysfunction after chemically induced menopause in mice. *Am. J. Physiol. Heart Circ. Physiol.* 323 (5), H845–H860. doi:10.1152/ajpheart.00276.2022

Blasco Tavares Pereira Lopes, F., Schlatzer, D., Wang, R., Li, X., Feng, E., Koyutürk, M., et al. (2022). Temporal and sex-linked protein expression dynamics in a familial model of alzheimer's disease. *Mol. Cell Proteomics* 21 (9), 100280. doi:10.1016/j.mcpro.2022.100280

Bohmbach, K., Masala, N., Schönhense, E. M., Hill, K., Haubrich, A. N., Zimmer, A., et al. (2022). An astrocytic signaling loop for frequency-dependent control of dendritic integration and spatial learning. *Nat. Commun.* 13 (1), 7932. doi:10.1038/s41467-022-35620-8

Bosson, A., Paumier, A., Boisseau, S., Jacquier-Sarlin, M., Buisson, A., and Albrieux, M. (2017). TRPA1 channels promote astrocytic Ca(2+) hyperactivity and synaptic dysfunction mediated by oligomeric forms of amyloid-β peptide. *Mol. Neurodegener.* 12 (1), 53. doi:10.1186/s13024-017-0194-8

Braak, H., and Braak, E. (1991). Neuropathological stageing of Alzheimer-related changes. *Acta Neuropathol.* 82 (4), 239–259. doi:10.1007/bf00308809

Brooks, H. L., Pollow, D. P., and Hoyer, P. B. (2016). The VCD mouse model of menopause and perimenopause for the study of sex differences in cardiovascular disease and the metabolic syndrome. *Physiol. (Bethesda)* 31 (4), 250–257. doi:10.1152/physiol.00057.2014

Bundy, J. L., Vied, C., Badger, C., and Nowakowski, R. S. (2019). Sex-biased hippocampal pathology in the 5XFAD mouse model of Alzheimer's disease: a multi-omic analysis. *J. Comp. Neurol.* 527 (2), 462–475. doi:10.1002/cne.24551

Cembrowski, M. S., Bachman, J. L., Wang, L., Sugino, K., Shields, B. C., and Spruston, N. (2016). Spatial gene-expression gradients underlie prominent heterogeneity of CA1 pyramidal neurons. *Neuron* 89 (2), 351–368. doi:10.1016/j.neuron.2015.12.013

Chowen, J. A., and Garcia-Segura, L. M. (2021). Role of glial cells in the generation of sex differences in neurodegenerative diseases and brain aging. *Mech. Ageing Dev.* 196, 111473. doi:10.1016/j.mad.2021.111473

Cinalli, D. A., Jr., Cohen, S. J., Calubag, M., Oz, G., Zhou, L., and Stackman, R. W., Jr. (2023). DREADD-inactivation of dorsal CA1 pyramidal neurons in mice impairs retrieval of object and spatial memories. *Hippocampus* 33 (1), 6–17. doi:10.1002/hipo.23484

Cornell, J., Salinas, S., Huang, H. Y., and Zhou, M. (2022). Microglia regulation of synaptic plasticity and learning and memory. *Neural Regen. Res.* 17 (4), 705–716. doi:10.4103/1673-5374.322423

Courtney, C. D., Sobieski, C., Ramakrishnan, C., Ingram, R. J., Wojnowski, N. M., DeFazio, R. A., et al. (2023). Optoα1AR activation in astrocytes modulates basal hippocampal synaptic excitation and inhibition in a stimulation-specific manner. *Hippocampus* 33 (12), 1277–1291. doi:10.1002/hipo.23580

Davis, J., Xu, F., Deane, R., Romanov, G., Previti, M. L., Zeigler, K., et al. (2004). Early-onset and robust cerebral microvascular accumulation of amyloid beta-protein in transgenic mice expressing low levels of a vasculotropic Dutch/Iowa mutant form of amyloid beta-protein precursor. *J. Biol. Chem.* 279 (19), 20296–20306. doi:10.1074/jbc.M312946200

Dong, Q., Kim, J., Nguyen, L., Bu, Q., and Chang, Q. (2020). An astrocytic influence on impaired tonic inhibition in hippocampal CA1 pyramidal neurons in a mouse model of rett syndrome. *J. Neurosci.* 40 (32), 6250–6261. doi:10.1523/jneurosci.3042-19.2020

Flurkey, K., and Currer, J. M. (2004). Pitfalls of animal model systems in ageing research. *Best. Pract. Res. Clin. Endocrinol. Metab.* 18 (3), 407–421. doi:10.1016/j.beem.2004.02.001

Ganesh, A., Choudhury, W., and Coutellier, L. (2024). Early spatial recognition memory deficits in 5XFAD female mice are associated with disruption of prefrontal parvalbumin neurons. *Brain Res.* 1841, 149122. doi:10.1016/j.brainres.2024.149122

Gannon, O. J., Naik, J. S., Riccio, D., Mansour, F. M., Abi-Ghanem, C., Salinero, A. E., et al. (2023). Menopause causes metabolic and cognitive impairments in a chronic cerebral hypoperfusion model of vascular contributions to cognitive impairment and dementia. *Biol. Sex. Differ.* 14 (1), 34. doi:10.1186/s13293-023-00518-7

Golub, M. S., Germann, S. L., Mercer, M., Gordon, M. N., Morgan, D. G., Mayer, L. P., et al. (2008). Behavioral consequences of ovarian atrophy and estrogen replacement in the APPswe mouse. *Neurobiol. aging* 29 (10), 1512–1523. doi:10.1016/j.neurobiolaging.2007.03.015

Gong, J., Harris, K., Peters, S. A. E., and Woodward, M. (2022). Reproductive factors and the risk of incident dementia: a cohort study of UK Biobank participants. *PLoS Med.* 19 (4), e1003955. doi:10.1371/journal.pmed.1003955

Haas, J. R., Christian, P. J., and Hoyer, P. B. (2007). Effects of impending ovarian failure induced by 4-vinylcyclohexene diepoxide on fertility in C57BL/6 female mice. *Comp. Med.* 57 (5), 443–449.

Habashi, M., Vutla, S., Tripathi, K., Senapati, S., Chauhan, P. S., Haviv-Chesner, A., et al. (2022). Early diagnosis and treatment of Alzheimer's disease by targeting toxic soluble Aβ oligomers. *Proc. Natl. Acad. Sci. U. S. A.* 119 (49), e2210766119. doi:10.1073/pnas.2210766119

Harsh, V., Schmidt, P. J., and Rubinow, D. R. (2007). The menopause transition: the next neuroendocrine frontier. *Expert Rev. Neurother.* 7 (11 Suppl. l), S7–S10. doi:10.1586/14737175.7.11s.S7

Hemond, P., Migliore, M., Ascoli, G. A., and Jaffe, D. B. (2009). The membrane response of hippocampal CA3b pyramidal neurons near rest: heterogeneity of passive properties and the contribution of hyperpolarization-activated currents. *Neuroscience* 160 (2), 359–370. doi:10.1016/j.neuroscience.2009.01.082

Heneka, M. T., Carson, M. J., El Khoury, J., Landreth, G. E., Brosseron, F., Feinstein, D. L., et al. (2015). Neuroinflammation in Alzheimer's disease. *Lancet Neurol.* 14 (4), 388–405. doi:10.1016/s1474-4422(15)70016-5

Hof, P., Young, W., Bloom, F., Belinchenko, P., and Ceilo, M. (2000). *Comparative cytoarchitectonic atlas of the C57BL/6 and 129/SV mouse brains*. 1 ed. Amsterdam: Elsevier.

Imai, Y., Ibata, I., Ito, D., Ohsawa, K., and Kohsaka, S. (1996). A novel gene iba1 in the major histocompatibility complex class III region encoding an EF hand protein expressed in a monocytic lineage. *Biochem. Biophys. Res. Commun.* 224 (3), 855–862. doi:10.1006/bbrc.1996.1112

Islam, R., Rajan, R., Choudhary, H., Vrionis, F., and Hanafy, K. A. (2024). Gender differences in Alzheimer's may be associated with TLR4-LYN expression in damage associated microglia and neuronal phagocytosis. *J. Cell Physiol.* 239 (6), e30916. doi:10.1002/jcp.30916

Kerchner, G. A., Deutsch, G. K., Zeineh, M., Dougherty, R. F., Saranathan, M., and Rutt, B. K. (2012). Hippocampal CA1 apical neuropil atrophy and memory performance in Alzheimer's disease. *Neuroimage* 63 (1), 194–202. doi:10.1016/j.neuroimage.2012.06.048

Kolahchi, Z., Henkel, N., Eladawi, M. A., Villarreal, E. C., Kandimalla, P., Lundh, A., et al. (2024). Sex and gender differences in alzheimer's disease: genetic, hormonal, and inflammation impacts. *Int. J. Mol. Sci.* 25 (15), 8485. doi:10.3390/ijms25158485

Kövari, E., Herrmann, F. R., Hof, P. R., and Bouras, C. (2013). The relationship between cerebral amyloid angiopathy and cortical microinfarcts in brain ageing and Alzheimer's disease. *Neuropathol. Appl. Neurobiol.* 39 (5), 498–509. doi:10.1111/nan.12003

Kubota, T., Matsumoto, H., and Kirino, Y. (2016). Ameliorative effect of membrane-associated estrogen receptor G protein coupled receptor 30 activation on object recognition memory in mouse models of Alzheimer's disease. *J. Pharmacol. Sci.* 131 (3), 219–222. doi:10.1016/j.jphs.2016.06.005

Laws, K. R., Irvine, K., and Gale, T. M. (2016). Sex differences in cognitive impairment in Alzheimer's disease. *World J. Psychiatry* 6, 54–65. doi:10.5498/wjp.v6.i1.54

Lei, D. L., Long, J. M., Hengemihle, J., O'Neill, J., Manaye, K. F., Ingram, D. K., et al. (2003). Effects of estrogen and raloxifene on neuroglia number and morphology in the hippocampus of aged female mice. *Neuroscience* 121 (3), 659–666. doi:10.1016/s0306-4522(03)00245-8

Lei, Z., Deng, P., Li, J., and Xu, Z. C. (2012). Alterations of A-type potassium channels in hippocampal neurons after traumatic brain injury. *J. Neurotrauma* 29 (2), 235–245. doi:10.1089/neu.2010.1537

Liao, H., Cheng, J., Pan, D., Deng, Z., Liu, Y., Jiang, J., et al. (2023). Association of earlier age at menopause with risk of incident dementia, brain structural indices and the potential mediators: a prospective community-based cohort study. *EClinicalMedicine* 60, 102033. doi:10.1016/j.eclinm.2023.102033

Lista, S., Imbimbo, B. P., Grasso, M., Fidilio, A., Emanuele, E., Minoretti, P., et al. (2024). Tracking neuroinflammatory biomarkers in Alzheimer's disease: a strategy for individualized therapeutic approaches? *J. Neuroinflammation* 21 (1), 187. doi:10.1186/s12974-024-03163-y

Liu, C. Y., Yang, Y., Ju, W. N., Wang, X., and Zhang, H. L. (2018). Emerging roles of astrocytes in neuro-vascular unit and the tripartite synapse with emphasis on reactive gliosis in the context of alzheimer's disease. *Front. Cell Neurosci.* 12, 193. doi:10.3389/fncel.2018.00193

Lohff, J. C., Christian, P. J., Marion, S. L., Arrandale, A., and Hoyer, P. B. (2005). Characterization of cyclicity and hormonal profile with impending ovarian failure in a

novel chemical-induced mouse model of perimenopause. *Comp. Med.* 55 (6), 523–527. Available online at: http://www.ncbi.nlm.nih.gov/pubmed/16422148.

Lu, Y., Sareddy, G. R., Wang, J., Zhang, Q., Tang, F. L., Pratap, U. P., et al. (2020). Neuron-Derived estrogen is critical for astrocyte activation and neuroprotection of the ischemic brain. *J. Neurosci.* 40 (38), 7355–7374. doi:10.1523/jneurosci.0115-20.2020

Ma, Y., Guo, H., Zhang, L., Tao, L., Yin, A., Liu, Z., et al. (2016). Estrogen replacement therapy-induced neuroprotection against brain ischemia-reperfusion injury involves the activation of astrocytes via estrogen receptor β. *Sci. Rep.* 6, 21467. doi:10.1038/srep21467

Ma, Y. L., Qin, P., Feng, D. Y., Li, Y., Zhang, L. X., Liu, Z. Y., et al. (2014). Estrogen regulates the expression of Ndrg2 in astrocytes. *Brain Res.* 1569, 1–8. doi:10.1016/j.brainres.2014.04.036

Maarouf, C. L., Kokjohn, T. A., Whiteside, C. M., Macias, M. P., Kalback, W. M., Sabbagh, M. N., et al. (2013). Molecular differences and similarities between alzheimer's disease and the 5XFAD transgenic mouse model of amyloidosis. *Biochem. Insights* 6, 1–10. doi:10.4137/bci.s13025

Manji, Z., Rojas, A., Wang, W., Dingledine, R., Varvel, N. H., and Ganesh, T. (2019). 5xFAD mice display sex-dependent inflammatory gene induction during the prodromal stage of alzheimer's disease. *J. Alzheimers Dis.* 70 (4), 1259–1274. doi:10.3233/jad-180678

Marazuela, P., Paez-Montserrat, B., Bonaterra-Pastra, A., Solé, M., and Hernández-Guillamon, M. (2022). Impact of cerebral amyloid angiopathy in two transgenic mouse models of cerebral β-amyloidosis: a neuropathological study. *Int. J. Mol. Sci.* 23 (9), 4972. doi:10.3390/ijms23094972

Marques-Lopes, J., Tesfaye, E., Israilov, S., Van Kempen, T. A., Wang, G., Glass, M. J., et al. (2017). Redistribution of NMDA receptors in estrogen-receptor-β-containing paraventricular hypothalamic neurons following slow-pressor angiotensin II hypertension in female mice with accelerated ovarian failure. *Neuroendocrinology* 104 (3), 239–256. doi:10.1159/000446073

Marques-Lopes, J., Van Kempen, T. A., and Milner, T. A. (2018). Rodent models of ovarian failure, in *Conn's handbook of models for human aging*, Ram Ed., 2nd ed.: Elsevier Inc., ch. Chapter 60, pp. 831–843.

Matafora, V., Gorb, A., Yang, F., Noble, W., Bachi, A., Perez-Nievas, B. G., et al. (2023). Proteomics of the astrocyte secretome reveals changes in their response to soluble oligomeric Aβ. *J. Neurochem.* 166 (2), 346–366. doi:10.1111/jnc.15875

Mayer, L. P., Devine, P. J., Dyer, C. A., and Hoyer, P. B. (2004). The follicle-deplete mouse ovary produces androgen. *Biol. Reprod.* 71 (1), 130–138. doi:10.1095/biolreprod.103.016113

Mills, Z. B., Faull, R. L. M., and Kwakowsky, A. (2023). Is hormone replacement therapy a risk factor or a therapeutic option for alzheimer's disease? *Int. J. Mol. Sci.* 24 (4), 3205. doi:10.3390/ijms24043205

Milner, T. A., Chen, R. X., Welington, D., Rubin, B. R., Contoreggi, N. H., Johnson, M. A., et al. (2022). Angiotensin II differentially affects hippocampal glial inflammatory markers in young adult male and female mice. *Learn Mem.* 29 (9), 265–273. doi:10.1101/lm.053507.121

Milner, T. A., Waters, E. M., Robinson, D. C., and Pierce, J. P. (2011). "Degenerating processes identified by electron microscpic immunocytochemical methods," in *Neurodegeneration, methods and protocols*. Editors G. Manfredi, and H. Kawamata (New York: Springer), 23–59.

Mitra, S. W., Hoskin, E., Yudkovitz, J., Pear, L., Wilkinson, H. A., Hayashi, S., et al. (2003). Immunolocalization of estrogen receptor beta in the mouse brain: comparison with estrogen receptor alpha. *Endocrinology* 144 (5), 2055–2067. doi:10.1210/en.2002-221069

Mitterling, K. L., Spencer, J. L., Dziedzic, N., Shenoy, S., McCarthy, K., Waters, E. M., et al. (2010). Cellular and subcellular localization of estrogen and progestin receptor immunoreactivities in the mouse hippocampus. *J. Comp. Neurol.* 518 (14), 2729–2743. doi:10.1002/cne.22361

Mosconi, L., Berti, V., Quinn, C., McHugh, P., Petrongolo, G., Varsavsky, I., et al. (2017). Sex differences in Alzheimer risk: brain imaging of endocrine vs chronologic aging. *Neurology* 89 (13), 1382–1390. doi:10.1212/wnl.0000000000004425

Mosconi, L., Rahman, A., Diaz, I., Wu, X., Scheyer, O., Hristov, H. W., et al. (2018). Increased Alzheimer's risk during the menopause transition: a 3-year longitudinal brain imaging study. *PLoS One* 13 (12), e0207885. doi:10.1371/journal.pone.0207885

Niwa, K., Kazama, K., Younkin, L., Younkin, S. G., Carlson, G. A., and Iadecola, C. (2002). Cerebrovascular autoregulation is profoundly impaired in mice overexpressing amyloid precursor protein. *Am. J. Physiol. Heart Circ. Physiol.* 283 (1), H315–H323. doi:10.1152/ajpheart.00022.2002

Oakley, H., Cole, S. L., Logan, S., Maus, E., Shao, P., Craft, J., et al. (2006). Intraneuronal beta-amyloid aggregates, neurodegeneration, and neuron loss in transgenic mice with five familial Alzheimer's disease mutations: potential factors in amyloid plaque formation. *J. Neurosci.* 26 (40), 10129–10140. doi:10.1523/JNEUROSCI.1202-06.2006

O'Leary, T. P., Stover, K. R., Mantolino, H. M., Darvesh, S., and Brown, R. E. (2020). Intact olfactory memory in the 5xFAD mouse model of Alzheimer's disease from 3 to 15 months of age. *Behav. Brain Res.* 393, 112731. doi:10.1016/j.bbr.2020.112731

Ortinski, P. I., Dong, J., Mungenast, A., Yue, C., Takano, H., Watson, D. J., et al. (2010). Selective induction of astrocytic gliosis generates deficits in neuronal inhibition. *Nat. Neurosci.* 13 (5), 584–591. doi:10.1038/nn.2535

Padurariu, M., Ciobica, A., Mavroudis, I., Fotiou, D., and Baloyannis, S. (2012). Hippocampal neuronal loss in the CA1 and CA3 areas of Alzheimer's disease patients. *Psychiatr. Danub* 24 (2), 152–158.

Park, L., Anrather, J., Forster, C., Kazama, K., Carlson, G. A., and Iadecola, C. (2004). Abeta-induced vascular oxidative stress and attenuation of functional hyperemia in mouse somatosensory cortex. *J. Cereb. Blood Flow. Metab.* 24 (3), 334–342. doi:10.1097/01.wcb.0000105800.49957.1e

Park, L., Hochrainer, K., Hattori, Y., Ahn, S. J., Anfray, A., Wang, G., et al. (2020). Tau induces PSD95-neuronal NOS uncoupling and neurovascular dysfunction independent of neurodegeneration. *Nat. Neurosci.* 23 (9), 1079–1089. doi:10.1038/s41593-020-0686-7

Park, L., Zhou, P., Pitstick, R., Capone, C., Anrather, J., Norris, E. H., et al. (2008). Nox2-derived radicals contribute to neurovascular and behavioral dysfunction in mice overexpressing the amyloid precursor protein. *Proc. Natl. Acad. Sci. U. S. A.* 105 (4), 1347–1352. doi:10.1073/pnas.0711568105

Phelan, K. D., Shwe, U. T., Wu, H., and Zheng, F. (2024). Investigating contributions of canonical transient receptor potential channel 3 to hippocampal hyperexcitability and seizure-induced neuronal cell death. *Int. J. Mol. Sci.* 25 (11), 6260. doi:10.3390/ijms25116260

Pierce, J. P., Kelter, D. T., McEwen, B. S., Waters, E. M., and Milner, T. A. (2014). Hippocampal mossy fiber leu-enkephalin immunoreactivity in female rats is significantly altered following both acute and chronic stress. *J. Chem. Neuroanat.* 55, 9–17. doi:10.1016/j.jchemneu.2013.10.004

Pike, C. J. (2017). Sex and the development of Alzheimer's disease. *J. Neurosci. Res.* 95, 671–680. doi:10.1002/jnr.23827

Pike, C. J. (1999). Estrogen modulates neuronal Bcl-xL expression and beta-amyloid-induced apoptosis: relevance to Alzheimer's disease. *J. Neurochem.* 72 (4), 1552–1563. doi:10.1046/j.1471-4159.1999.721552.x

Pirttimaki, T. M., Codadu, N. K., Awni, A., Pratik, P., Nagel, D. A., Hill, E. J., et al. (2013). α7 Nicotinic receptor-mediated astrocytic gliotransmitter release: aβ effects in a preclinical Alzheimer's mouse model. *PLoS One* 8 (11), e81828. doi:10.1371/journal.pone.0081828

Platholi, J., Marongiu, R., Park, L., Yu, F., Sommer, G., Weinberger, R., et al. (2023). Hippocampal glial inflammatory markers are differentially altered in a novel mouse model of perimenopausal cerebral amyloid angiopathy. *Front. Aging Neurosci.* 15, 1280218. doi:10.3389/fnagi.2023.1280218

Poon, C. H., Wong, S. T. N., Roy, J., Wang, Y., Chan, H. W. H., Steinbusch, H., et al. (2023). Sex differences between neuronal loss and the early onset of amyloid deposits and behavioral consequences in 5xFAD transgenic mouse as a model for alzheimer's disease. *Cells* 12 (5), 780. doi:10.3390/cells12050780

Prange-Kiel, J., Dudzinski, D. A., Pröls, F., Glatzel, M., Matschke, J., and Rune, G. M. (2016). Aromatase expression in the Hippocampus of AD patients and 5xFAD mice. *Neural Plast.* 2016, 9802086. doi:10.1155/2016/9802086

Prat, A., Behrendt, M., Marcinkiewicz, E., Boridy, S., Sairam, R. M., Seidah, N. G., et al. (2011). A novel mouse model of Alzheimer's disease with chronic estrogen deficiency leads to glial cell activation and hypertrophy. *J. Aging Res.* 2011, 251517. doi:10.4061/2011/251517

Prinz, M., Masuda, T., Wheeler, M. A., and Quintana, F. J. (2021). Microglia and central nervous system-associated macrophages-from origin to disease modulation. *Annu. Rev. Immunol.* 39, 251–277. doi:10.1146/annurev-immunol-093019-110159

Quinn, J. F., Kelly, M. J., Harris, C. J., Hack, W., Gray, N. E., Kulik, V., et al. (2022). The novel estrogen receptor modulator STX attenuates Amyloid-β neurotoxicity in the 5XFAD mouse model of Alzheimer's disease. *Neurobiol. Dis.* 174, 105888. doi:10.1016/j.nbd.2022.105888

Raz, L., Knoefel, J., and Bhaskar, K. (2016). The neuropathology and cerebrovascular mechanisms of dementia. *J. Cereb. Blood Flow. Metab.* 36 (1), 172–186. doi:10.1038/jcbfm.2015.164

Richard, B. C., Kurdakova, A., Baches, S., Bayer, T. A., Weggen, S., and Wirths, O. (2015). Gene dosage dependent aggravation of the neurological phenotype in the 5XFAD mouse model of alzheimer's disease. *J. Alzheimers Dis.* 45 (4), 1223–1236. doi:10.3233/jad-143120

Rune, G. M., Wehrenberg, U., Prange-Kiel, J., Zhou, L., Adelmann, G., and Frotscher, M. (2002). Estrogen up-regulates estrogen receptor alpha and synaptophysin in slice cultures of rat hippocampus. *Neuroscience* 113 (1), 167–175. doi:10.1016/s0306-4522(02)00152-5

Sadleir, K. R., Eimer, W. A., Cole, S. L., and Vassar, R. (2015). Aβ reduction in BACE1 heterozygous null 5XFAD mice is associated with transgenic APP level. *Mol. Neurodegener.* 10, 1. doi:10.1186/1750-1326-10-1

Sahambi, S. K., Visser, J. A., Themmen, A. P., Mayer, L. P., and Devine, P. J. (2008). Correlation of serum anti-Müllerian hormone with accelerated follicle loss following 4-vinylcyclohexene diepoxide-induced follicle loss in mice. *Reprod. Toxicol.* 26 (2), 116–122. doi:10.1016/j.reprotox.2008.07.005

Sakuma, S., Tokuhara, D., Hattori, H., Matsuoka, O., and Yamano, T. (2009). Expression of estrogen receptor alpha and beta in reactive astrocytes at the male rat

hippocampus after status epilepticus. *Neuropathology* 29 (1), 55–62. doi:10.1111/j.1440-1789.2008.00946.x

Santos-Galindo, M., Acaz-Fonseca, E., Bellini, M. J., and Garcia-Segura, L. M. (2011). Sex differences in the inflammatory response of primary astrocytes to lipopolysaccharide. *Biol. Sex. Differ.* 2, 7. doi:10.1186/2042-6410-2-7

Sárvári, M., Kalló, I., Hrabovszky, E., Solymosi, N., and Liposits, Z. (2017). Ovariectomy alters gene expression of the hippocampal formation in middle-aged rats. *Endocrinology* 158 (1), 69–83. doi:10.1210/en.2016-1516

Sasaki, Y., Ohsawa, K., Kanazawa, H., Kohsaka, S., and Imai, Y. (2001). Iba1 is an actin-cross-linking protein in macrophages/microglia. *Biochem. Biophys. Res. Commun.* 286 (2), 292–297. doi:10.1006/bbrc.2001.5388

Shughrue, P. J., and Merchenthaler, I. (2000). Evidence for novel estrogen binding sites in the rat hippocampus. *Neuroscience* 99 (4), 605–612. doi:10.1016/s0306-4522(00)00242-6

Sil, A., Erfani, A., Lamb, N., Copland, R., Riedel, G., and Platt, B. (2022). Sex differences in behavior and molecular pathology in the 5XFAD model. *J. Alzheimers Dis.* 85 (2), 755–778. doi:10.3233/jad-210523

Šišková, Z., Justus, D., Kaneko, H., Friedrichs, D., Henneberg, N., Beutel, T., et al. (2014). Dendritic structural degeneration is functionally linked to cellular hyperexcitability in a mouse model of Alzheimer's disease. *Neuron* 84 (5), 1023–1033. doi:10.1016/j.neuron.2014.10.024

Steventon, J. J., Lancaster, T. M., Baker, E. S., Bracher-Smith, M., Escott-Price, V., Ruth, K. S., et al. (2023). Menopause age, reproductive span and hormone therapy duration predict the volume of medial temporal lobe brain structures in postmenopausal women. *Psychoneuroendocrinology* 158, 106393. doi:10.1016/j.psyneuen.2023.106393

Stone, D. J., Song, Y., Anderson, C. P., Krohn, K. K., Finch, C. E., and Rozovsky, I. (1998). Bidirectional transcription regulation of glial fibrillary acidic protein by estradiol *in vivo* and *in vitro*. *Endocrinology* 139 (7), 3202–3209. doi:10.1210/endo.139.7.6084

Sun, Q., Sotayo, A., Cazzulino, A. S., Snyder, A. M., Denny, C. A., and Siegelbaum, S. A. (2017). Proximodistal heterogeneity of hippocampal CA3 pyramidal neuron intrinsic properties, connectivity, and reactivation during memory recall. *Neuron* 95 (3), 656–672 e3. doi:10.1016/j.neuron.2017.07.012

Thompson, C. L., Pathak, S. D., Jeromin, A., Ng, L. L., MacPherson, C. R., Mortrud, M. T., et al. (2008). Genomic anatomy of the hippocampus. *Neuron* 60 (6), 1010–1021. doi:10.1016/j.neuron.2008.12.008

Tolar, M., Hey, J., Power, A., and Abushakra, S. (2021). Neurotoxic soluble amyloid oligomers drive alzheimer's pathogenesis and represent a clinically validated target for slowing disease progression. *Int. J. Mol. Sci.* 22 (12), 6355. doi:10.3390/ijms22126355

Tong, M. K., Thakur, A., Yang, T., Wong, S. K., Li, W. K., and Lee, Y. (2024). Amyloid-β oligomer-induced neurotoxicity by exosomal interactions between neuron and microglia. *Biochem. Biophys. Res. Commun.* 727, 150312. doi:10.1016/j.bbrc.2024.150312

Tsurugizawa, T., Mukai, H., Tanabe, N., Murakami, G., Hojo, Y., Kominami, S., et al. (2005). Estrogen induces rapid decrease in dendritic thorns of CA3 pyramidal neurons in adult male rat hippocampus. *Biochem. Biophys. Res. Commun.* 337 (4), 1345–1352. doi:10.1016/j.bbrc.2005.09.188

Turner, C. D., and Bagnara, J. T. (1971). *General endocrinology*. Philadelphia: W.B. Saunders.

Van Kempen, T. A., Gorecka, J., Gonzalez, A. D., Soeda, F., Milner, T. A., and Waters, E. M. (2014). Characterization of neural estrogen signaling and neurotrophic changes in the accelerated ovarian failure mouse model of menopause. *Endocrinology* 155 (9), 3610–3623. doi:10.1210/en.2014-1190

Van Kempen, T. A., Kahlid, S., Gonzalez, A. D., Spencer-Segal, J. L., Tsuda, M. C., Ogawa, S., et al. (2013). Sex and estrogen receptor expression influence opioid peptide levels in the mouse hippocampal mossy fiber pathway. *Neurosci. Lett.* 552, 66–70. doi:10.1016/j.neulet.2013.07.048

Van Kempen, T. A., Milner, T. A., and Waters, E. M. (2011). Accelerated ovarian failure: a novel, chemically induced animal model of menopause. *Brain Res.* 1379, 176–187. doi:10.1016/j.brainres.2010.12.064

Wang, Y., Fu, W. Y., Cheung, K., Hung, K. W., Chen, C., Geng, H., et al. (2021). Astrocyte-secreted IL-33 mediates homeostatic synaptic plasticity in the adult hippocampus. *Proc. Natl. Acad. Sci. U. S. A.* 118 (1), e2020810118. doi:10.1073/pnas.2020810118

Waters, E. M., Thompson, L. I., Patel, P., Gonzales, A. D., Ye, H. Z., Filardo, E. J., et al. (2015). G-protein-coupled estrogen receptor 1 is anatomically positioned to modulate synaptic plasticity in the mouse hippocampus. *J. Neurosci.* 35 (6), 2384–2397. doi:10.1523/jneurosci.1298-14.2015

Wedatilake, Y., Myrstad, C., Tom, S. E., Strand, B. H., Bergh, S., and Selbæk, G. (2024). Female reproductive factors and risk of mild cognitive impairment and dementia: the HUNT study. *J. Prev. Alzheimers Dis.* 11 (4), 1063–1072. doi:10.14283/jpad.2024.46

Weiland, N. G., Orikasa, C., Hayashi, S., and McEwen, B. S. (1997). Distribution and hormone regulation of estrogen receptor immunoreactive cells in the hippocampus of male and female rats. *J. Comp. Neurol.* 388 (4), 603–612. doi:10.1002/(sici)1096-9861(19971201)388:4<603::aid-cne8>3.0.co;2-6

Williams, T. J., and Milner, T. A. (2011). Delta opioid receptors colocalize with corticotropin releasing factor in hippocampal interneurons. *Neuroscience* 179, 9–22. doi:10.1016/j.neuroscience.2011.01.034

Williams, T. J., Torres-Reveron, A., Chapleau, J. D., and Milner, T. A. (2011). Hormonal regulation of delta opioid receptor immunoreactivity in interneurons and pyramidal cells in the rat hippocampus. *Neurobiol. Learn. Mem.* 95 (2), 206–220. doi:10.1016/j.nlm.2011.01.002

Wittner, L., and Miles, R. (2007). Factors defining a pacemaker region for synchrony in the hippocampus. *J. Physiol.* 584 (Pt 3), 867–883. doi:10.1113/jphysiol.2007.138131

Wright, L. E., Christian, P. J., Rivera, Z., Van Alstine, W. G., Funk, J. L., Bouxsein, M. L., et al. (2008). Comparison of skeletal effects of ovariectomy versus chemically induced ovarian failure in mice. *J. Bone Min. Res.* 23 (8), 1296–1303. doi:10.1359/jbmr.080309

Wu, K., Canning, K. J., and Leung, L. S. (1998). Functional interconnections between CA3 and the dentate gyrus revealed by current source density analysis. *Hippocampus* 8 (3), 217–230. doi:10.1002/(SICI)1098-1063(1998)8:3<217::AID-HIPO5>3.0.CO;2-G

Xu, F., Grande, A. M., Robinson, J. K., Previti, M. L., Vasek, M., Davis, J., et al. (2007). Early-onset subicular microvascular amyloid and neuroinflammation correlate with behavioral deficits in vasculotropic mutant amyloid beta-protein precursor transgenic mice. *Neuroscience* 146 (1), 98–107. doi:10.1016/j.neuroscience.2007.01.043

Xu, W., Xu, F., Anderson, M. E., Kotarba, A. E., Davis, J., Robinson, J. K., et al. (2014a). Cerebral microvascular rather than parenchymal amyloid-β protein pathology promotes early cognitive impairment in transgenic mice. *J. Alzheimers Dis.* 38 (3), 621–632. doi:10.3233/jad-130758

Xu, W., Xu, F., Anderson, M. E., Kotarba, A. E., Davis, J., Robinson, J. K., et al. (2014b). Cerebral microvascular rather than parenchymal amyloid-β protein pathology promotes early cognitive impairment in transgenic mice. *J. Alzheimers Dis.* 38, 621–632. doi:10.3233/JAD-130758

Yakemow, G., Kolesar, T. A., Wright, N., Beheshti, I., Choi, E. H., Ryner, L., et al. (2024). Investigating neural markers of Alzheimer's disease in posttraumatic stress disorder using machine learning algorithms and magnetic resonance imaging. *Front. Neurol.* 15, 1470727. doi:10.3389/fneur.2024.1470727

Zhang, J., Zhang, Y., Wang, J., Xia, Y., and Chen, L. (2024). Recent advances in Alzheimer's disease: mechanisms, clinical trials and new drug development strategies. *Signal Transduct. Target Ther.* 9 (1), 211. doi:10.1038/s41392-024-01911-3